Hindawi
Journal of Chemistry
Volume 2022, Article ID 7504626, 25 pages
https://doi.org/10.1155/2022/7504626

Review Article

Review of Clay-Based Nanocomposites as Adsorbents for the Removal of Heavy Metals

Ismael Kithinji Kinoti,[1] Esther Muthoni Karanja,[1] Esther Wanja Nthiga,[2] Cyprian Muturia M'thiruaine,[1] and Joseph Mwiti Marangu[1]

[1]*Physical Sciences, Meru University of Science and Technology, Meru, Kenya*
[2]*Department of Chemistry, Dedan Kimathi University of Technology, Nyeri, Kenya*

Correspondence should be addressed to Joseph Mwiti Marangu; jmarangu2011@gmail.com

Received 26 January 2022; Revised 6 May 2022; Accepted 11 May 2022; Published 22 June 2022

Academic Editor: Mehdi Vosoughi

Due to rapid industrialization, urbanization, and surge in modern human activities, water contamination is a major threat to humanity globally. Contaminants ranging from organic compounds, dyes, to inorganic heavy metals have been of major concern in recent years. This necessitates the development of affordable water remediation technologies to improve water quality. There is a growing interest in nanotechnology recently because of its application in eco-friendly, cost-effective, and durable material production. This study presents a review of recent nanocomposite technologies based on clay, applied in the removal of heavy metals from wastewater, and highlights the shortcomings of existing methods. Recently published reports, articles, and papers on clay-based nanocomposites for the removal of heavy metals have been reviewed. Currently, the most common methods utilized in the removal of heavy metals are reverse osmosis, electrodialysis, ion exchange, and activated carbon. These methods, however, suffer major shortcomings such as inefficiency when trace amounts of contaminant are involved, uneconomical costs of operation and maintenance, and production of contaminated sludge. The abundance of clay on the Earth's surface and the ease of modification to improve adsorption capabilities have made it a viable candidate for the synthesis of nanocomposites. Organoclay nanocomposites such as polyacrylamide-bentonite, polyaniline-montmorillonite, and β-cyclodextrin-bentonite have been synthesized for the selective removal of various heavy metals such as Cu^{2+}, Co^{2+}, among others. Bacterial clay nanocomposites such as *E. coli* kaolinite nanocomposites have also been successfully synthesized and applied in the removal of heavy metals. Low-cost nanocomposites of clay using biopolymers like chitosan and cellulose are especially in demand due to the cumulative abundance of these materials in the environment. A comparative analysis of different synthetic processes to efficiently remove heavy metal contaminants with clay-based nanocomposite adsorbents is made.

1. Introduction

Water is considered as the most essential source of life with its usage ranging from domestic consumption to industrial applications in cooling machinery and manufacturing. Globally, water makes up 71% of the Earth's surface, with a major part of it (95.5%) in the oceans [1]. In a publication by FAO-AQUASTAT, [2] it is estimated that by 2050, food and water will need to be provided to about 9-10 billion people, owing to a growing global population. The North American and European industries alone use about 50% of all water [3]. This is in comparison to 4 to 12% in developing countries. World Health Organization [4] outlines that about 785 million people do not have access to clean and safe water. About 37% of these people live in Sub-Saharan Africa. The same report outlines that 1 in 3 people worldwide does not have access to safe and clean drinking water, a state much more worsened when referencing children. More than 500,000 children die annually due to poor sanitation and unsafe or contaminated water [5]. Industrialization, modern agriculture, and other effects of human activities are the major sources of water contaminants (Philippines, [6]).

Wastewater, generally classified as domestic, industrial, or stormwater, has been defined as the used or polluted form

of water due to human activities or rainwater runoff [7]. The EPA [8] estimates that 23,000–75,000 sanitary sewers overflow each year, contaminating adjacent water sources. In addition to this, about 80% of global wastewater finds its way back to the ecosystem without undergoing any form of treatment [9]. This translates that close to 1.8 billion people globally utilize contaminated water sources. In Kenya, approximately 32% of the total population consumes water from water sources prone to contamination [10]. Industrial wastewater has been defined as the effluent resulting from substances suspended or dissolved in water after it has undergone a manufacturing process or cleaning activities involved in that process [11]. Very high volumes ranging from 3 to 10 billion gallons of sewerage effluents are released annually from treatment plants [12]. Industrial sewerage is estimated to account for approximately 22% of global water use, according to FAO-AQUASTAT [2]. In addition, approximately 80% of global municipal and industrial wastewater end up polluting the environment in untreated forms. Globally, public wastewater treatment facilities process more than 8 million tons of dry sludge annually, which consumes about a third of electricity use [13]. Lower middle-income countries are reported to treat only about 28% of their wastewater, which means that in most countries in Africa, about 72% of the sewerage effluents produced end up contaminating the environment, endangering human lives [10].

Wastewater effluents from factories are common heavy metal contaminants to the environment, especially if the effluents are not properly treated prior to disposal [14]. Heavy metals have been defined as metallic elements whose density is considerably higher than that of water and, in relatively low concentrations, exhibit toxicity or poisonous effects [15]. Some of these metals include lead (Pb), mercury (Hg), arsenic (As), thallium (Tl), and cadmium (Cd). Some heavy metals like gold exist naturally on Earth's crust and are often exploited for various applications. Others like manganese, iron, among others, play an important role in biochemical processes within the body, while they are present in trace amounts [16]. Bioaccumulation of heavy metals in the human body is what causes adverse effects as affecting the nervous system, kidneys, among others [17]. Heavy metals eventually find their way to human bodies as a result of anthropogenic activities like industrial waste release, mining activities, use of contaminated water for irrigation, among others. Most heavy metals exist as compounded salts in ores as sulfides or oxides. Copper, gold, and manganese are known to exist naturally as oxides. Silver, lead, and iron exist naturally as sulfides. When mined, these ores are blasted and heavy metals are released into the open environment, consequently finding their way into water bodies, air, and soil as effluents. In industries, paints, pesticides, herbicides, and cosmetics are common carriers of heavy metals that are exposed to the environment through erosion or runoff [16].

Heavy metals have diverse effects when they bioaccumulate in human bodies. Arsenic, in an inorganic state, occurs as arsenate and arsenite. Major sources of this metal include microelectronic industries and smelting zones. Other sources include paints, wood preservatives, and pesticides [18]. Arsenic bioaccumulates in nails, hair, and the skin when it gets into the body. In some instances, it is transported through the bloodstream to accumulate in the heart, liver, neural tissues, and kidney [16]. The mechanism of the biological toxicity of arsenic is not clear. It is however reported that it generates free radicals like the peroxyl *radical* ($ROO^{\cdot}$), dimethyl *arsenic radical* ($(CH_3)_2As\cdot$), *superoxide* ($O_2\cdot$), *nitric oxide* (NO•), *singlet oxygen* ($^1O_2$), among others [19]. Lead is one of the flagged heavy metals for acute environmental poisoning today [20]. Major sources of lead are linked to cigarettes, and domestic and industrial sources. Storage batteries, gasoline, paints, and some plumbing pipes have been documented as some major sources of lead contamination [17]. Once it finds its way to human bodies, lead can induce carcinogenic processes that have been reported to cause DNA damage and interfere with the DNA repair processes through the generation of reactive oxygen species [20]. Cadmium is widely distributed on the Earth's surface and is estimated to have an average concentration of about 0.1 mg/kg [21]. Applications of this metal include the production of batteries, alloys, and pigments [22]. Due to strict environmental regulations, cadmium uptake has been on the decrease especially in developed countries. In the United States, the daily uptake of cadmium has been reported to be about 0.4 ug/kg, which is less than half of the U.S. EPA oral reference dose (US, [8]). Exposure to cadmium occurs through occupational exposure like working in cadmium-contaminated industries, smoking cigarettes, or eating contaminated food. In some foods, cadmium is found in trace amounts like in leafy vegetables, liver and kidney, dried seaweed, among others [21]. Exposure is determined through blood samples or urine analysis, with cigarette smokers estimated to have the highest cadmium levels in both samples [23]. Symptoms associated with cadmium exposure include nausea, abdominal pain, muscle cramps, burning sensation, shock, and in severe cases, loss of consciousness within 15 to 30 minutes [21].

In this regard, different methods have been employed in the remediation of heavy metals from wastewater. Clay-based nanocomposites have recently gained much attention in the removal of heavy metals due to their increased surface area and modifiable structures for selective contaminant removal [24]. The removal of various heavy metals, by various clay-based nanocomposites, is discussed in this review.

2. Wastewater

2.1. Components of Wastewater. Wastewater is made up of major components that are related to the treatment processes employable on the sewage [25]. Some of these components include biochemical oxygen demand (BOD), total suspended solids (TSSs), pathogens, nutrients, and other emergent contaminants [25]. BOD is described as the amount of oxygen required or demanded by organic compounds in wastewater to break down into simple and stable compounds. A high BOD dictates that wastewater

microbes would compete for oxygen with marine life if such effluent is released to water bodies. It is of importance to reduce BOD before the wastewater is released into water bodies. The EPA standard concentration for BOD is 50 mg/L [26]. However, different countries have their respective allowable standard values of BOD for wastewater. Unpolluted water typically has a BOD concentration of approximately 1 mg/L [27]. Household wastewater is typically in the range of 200 mg/L for BOD [25]. This means that, under standard procedures, it would take approximately 200 mg of dissolved oxygen to break down its organic matter in approximately 5 days. Values in the range of 200–600 mg/L have the water considered polluted and must be processed before releasing to the environment [27]. According to Bezsenyi et al. [28], the effect of hydrogen peroxide on the values of BOD measured during ionizing radiation treatment of wastewater can be erroneously overestimated in the presence of high concentrations of hydrogen peroxide. In a study conducted by Skoczko et al. [29] investigating the influence of seasonal changes on various wastewater factors, it was reported that the values of BOD removal efficiency showed no significant difference over the seasons. However, the removal efficiency increased slightly from winter to summer due to the positive change in temperature. Nezhadheydari et al. [30] investigated the effect of magnetic nanoparticle concentrations on aquaculture wastewater treatment. The study reported that the effect of the nanoparticles on BOD was only significant at high concentrations. Pavithra and Shanthakumar [31] reported BOD removal of 62.7% and 57.27% when using silica and iron nanoparticles, respectively, from aquaculture wastewater. Gharloghi et al. [32] estimated that iron oxide nanoparticles could reduce BOD by approximately 25% when applied to municipal wastewater.

TSS is the number of solids of a specific size (more than 2 microns) dispersed in the wastewater in suspension. It is the specific measurement of the total suspended mass of solid material in wastewater, whether organic or inorganic. Any particles less than 2 microns in size are considered dissolved solids [33]. In the environment, they are capable of clogging fish gills, smothering fish eggs, and decreasing light dispersion in water bodies. They can be organic, such as fecal matter, or inorganic, such as silt or clay. A high value of TSS indicates a high biological oxygen demand, meaning that a high percentage of solids is organic matter [25]. Often, turbidity measurements are an estimate, and not an exact value, of TSS. Turbidity is the optical determination of the clarity of water, that is affected by both the dissolved matter and the suspended particles in a water column [8]. Turbidity values indicate the change in TSS concertation of wastewater without giving exact measurements [34]. In most cases, TSS values below 20 mg/L will show low turbidity levels of about 5 NTU, which is visually clear. TSS levels over 40 mg/L shows cloudiness, which in comparison to estimated turbidity levels show a value of about 55 NTU [35]. Raw wastewater will often have TSS in the range of 155–330 mg/L, whereby 250 mg/L is considered a typical wastewater TSS concentration. After the primary treatment stage, this value is expected to fall below 65 mg/L and below 25 mg/L after the advanced secondary treatment system [36]. TSS-contaminated wastewater increases the TSS value of waterbodies it may be dumped into. When this happens, the rise in TSS value can contribute to a rise in water temperature and consequently decrease in dissolved oxygen (DO) [34]. This happens when radiant heat from the sunlight is absorbed by suspended matter that heats the water molecules by conduction. Warmer waters release oxygen easier than colder waters; therefore, this process lowers the levels of DO [37]. In addition, high TSS levels can induce water stratification, whereby water layers themselves by temperature zones in such a way that the colder layers (bottom) do not intermix with warmer layers (top). Since respiration and decomposition occur in the lower layers, the lack of intermiscibility would cause a state of hypoxia when gradually decreasing oxygen levels to make it challenging for organisms to survive [33]. In a study conducted by Amerian et al. [38], studying the effect of TSS, among other factors, on peracetic acid (PAA) decomposition, it was reported that PAA demand increased for both primary and secondary effluents with increase in concentration of TSS. The higher demand for PAA in primary effluent was attributed to a higher concentration of suspended organic matter. The observed decay rate was 0.014 L/mg·min and 0.0039 L/mg·min in primary and secondary effluents, respectively, for every 10 mg/L increase in TSS concentration. The higher decay rate in primary effluent was also attributed to a higher concentration of organic matter in primary effluent. In a similar study by, PAA rate of decay was observed to increase by a factor of five as the concentration of TSS increased gradually from 40 to 160 mg/L.

2.2. Characteristics of Wastewater and Effluent Quality Parameters. Wastewater is characterized into three major groups, namely physical, chemical, and biological characteristics [39]. The physical characteristics include the color, turbidity, temperature, odor, and total solids in the wastewater. Sewer water is often brown and yellow when fresh, and turns to dark color in time, as the organic matter begins to decay [40]. It is a common characteristic of sewer effluents to have a strong pungent odor. Temperatures are always higher than normal due to biological activities that occur in the sewer water. Additionally, the turbidity of sewerage is high due to a high percentage of suspended solids [41].

Chemical characteristics include nitrogen, chemical oxygen demand (COD), alkalinity, pH, total organic carbon (TOC), chlorides, heavy metals, phosphorus, among others [42]. COD defines the organic matter in wastewater by determining the amount of oxygen required to oxidize them. It is the quantity of oxygen that must be in the water to oxidize the embedded chemical organic pollutants. High levels of COD could indicate an imminent decrease in dissolved oxygen, which can negatively impact marine life and balance [43]. The TOC describes the amount of carbon embedded in the organic materials in the wastewater. This parameter is usually investigated as an ongoing assessment of the change or lack of change of the organic content in the wastewater [44]. Whitehead argued that TOC on its own does not give satisfactory data regarding the organic content

in wastewater as compounds containing carbon can exist in different forms. Phosphorus can exist both organically and inorganically in wastewater. Nitrogen is often found in organic forms in wastewater.

The biological characteristics include bacteria, fungi, algae, viruses, and protozoa [41]. In the sewage, both intestinal and sewage bacteria are found. Pathogenic and nonpathogenic intestinal bacteria such as fecal coliform, *Salmonella, Vibrio cholera,* among others, find their way to sewers through human stool. Anaerobic and aerobic sewage bacteria exist naturally in sewer systems, playing a key role in breaking down organic matter. *Pepto coccus, Bifidobacterium, Nocardia, Achromobactin,* among others, are some of the common real sewage bacteria. Algae and fungi in sewerage effluents play an important role in trickling filters during sewage treatment [41].

2.3. Wastewater Treatment. Edwards [11] classified wastewater treatment methods into physical/chemical, thermal, and biological classes. As the class names dictate, physical/chemical methods employ the physical or chemical properties of the wastewater constituents to effect ample change in the composition. Thermal methods involve the use of heat that decomposes pollutants, while biological methods involve the use of microorganisms in the removal of undesirable wastes. In wastewater treatment, however, three major steps, namely primary, secondary, and tertiary, are undertaken to ensure clean and safe water [45].

Primary treatment, also known as a preliminary treatment, involves the removal of grit and screenings from the wastewater, often by the use of physical methods [46]. Primary sanitation technology reduces suspended solids through the removal of scum and suspended solids through surface screening and gravity settling. Bar screens are used for the screening step and gravity settling makes use of grit chambers to remove the settled grit [47]. Secondary treatment is usually standardized to remove dissolved organic matter that is not caught by the primary treatment stage and suspended solids [7]. Biological processes play a key role in waste removal at this stage, as microorganisms metabolize organic matter to energy, water, and carbon dioxide. The methods employed at this stage are trickling filters, oxidation ponds, and activated sludge processes [45]. Recently, a rotating biocontacter has been used [7]. Activated sludge process, being the most common method in developing countries, has been reported to remove approximately 80% BOD and 78.28% COD in attached and suspended growth reactors [48]. Tertiary processes are usually employed in cases where the quality of the remediated water is of utmost importance. Therefore, tertiary methods polish secondary effluents to reduce unsafe concentrations of dissolved chemicals such as heavy metals, phosphates, and nitrates [45]. Granular media filters and micro-strainers are used to remove BOD and any suspended solids from secondary effluents in a process known as effluent polishing [49, 50]. These steps are summarized in Figure 1. Percentage removal efficiencies of different pollutants at different stages are summarized in Table 1 [53].

In developing countries, the primary and the secondary treatment stages are the most common in the municipal wastewater process. This is due to the high maintenance costs involved in setting up modern tertiary treatment facilities, which often leave their application to private companies. The existing methods applied in the primary and secondary stages such as the activated sludge process do not particularly address the removal of heavy metals. This means that most wastewater effluents from the primary and secondary treatment contain heavy metal concentrations dangerous to the environment, animals, and humans alike. Sustainable and affordable technologies such as clay-based nanocomposites are being looked into to address this problem, especially in developing countries whereby modern tertiary wastewater remediation methods are expensive to set up and maintain.

3. Techniques of Heavy Metal Decontamination

3.1. Metal Precipitation. Metal precipitation methods remove metals from wastewater by converting the metal ion from the dissolved state to a solid state that is precipitated. These methods employ chemical additives or make use of microbiological processes. The most important parameter in these methods is that the concentration of the metal ion has to be high in complex liquid states. Metal precipitation techniques do not achieve complete metal ion removal, and often multiple techniques are employed in addition to removing the metal ions [54].

3.1.1. Chemical Precipitation. Chemical precipitation works under the metal ion saturation principle. When a solution becomes saturated with metal ions and the solubility product (Ksp) of the system is exceeded, the metal ion is precipitated [55]. Ksp is the product at equilibrium between a solid and its ions in the solution. The stages followed by a precipitation process include the nucleation stage, nucleus growth, and then the crystallization or aggregation stage [54]. Factors that affect the quality of the precipitation process include the concentration of the metal ions of interest, their type, the conditions of the reaction like pH, the type of precipitant used, and most importantly, the availability of precipitation inhibitors [56].

Hydroxide precipitation employs alteration in pH using calcium hydroxide or sodium hydroxide as the precipitation agent. Different metals have optimal pH values for the optimum hydroxide precipitation to occur, mainly in the range of 7.5 to 11. The main challenge for this method is that most metallic hydroxides exhibit amphoteric behavior, which imposes a different challenge on precipitated metals to solubilize back into the solution [56]. In addition to this limitation, this method is prone to problematic sludge that needs further processing. Wang and Chen [57] proposed a method to sequentially precipitate heavy metals (Fe, Cu, and Zn) and treat the sludge concurrently by modifying the hydroxide precipitation with sulfide precipitation and oxidation treatment. In this manner, they achieved 99.8% Fe removal, 94% Cu removal, and 96.1% Zn removal and an

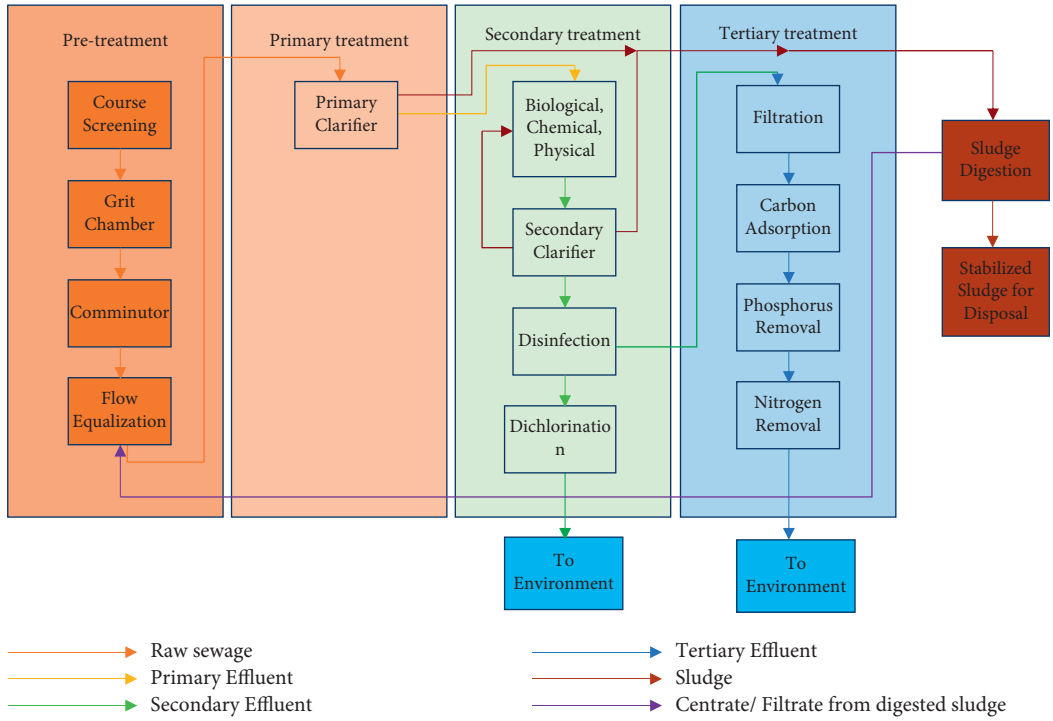

Figure 1: Summary of wastewater treatment steps.

Table 1: Percentage removal of pollutants at different stages.

Stage	Method	% Removal					References
		COD/BOD	TSS	Pathogens	Nitrogen	Phosphorus	
Primary	Sedimentation	45%	70%	—	0–35%	0–35%	[46]
	Fine screen	45%	—	—	—	—	
Secondary	Primary clarifier	30.59%	50.61%	—	—	—	[51, 52]
	Aeration tanks	73%	80%	75%	60%	50%	
	Activated sludge	91.28%	86.76%	50–80%	>70%	>70%	
Tertiary	Activated carbon	85%	52%	95%	50%	60%	[52]
	Ion exchange	70–95%	35–85%	>80%	35–80%	35–80%	
	Disinfection	—	—	98%	—	—	

increasing need for sludge disposal. In a study by Li et al. [58], hydroxide precipitation method was used in the recovery of Zn ions achieving 70–80% removal, in a combined Fenton process.

Sulfide precipitation provides less soluble metal precipitates and offers potential for selectivity in heavy metal removal. This method is however used sparingly, due to difficulties in controlling sulfide dosage and dangers of toxicity in the case of excess sulfide. This form of precipitation can be achieved by the use of solid iron sulfide or calcium sulfide, aqueous ammonium sulfide, sodium sulfide or sodium hydrogen sulfide, or gaseous hydrogen sulfide [59]. Zainuddin et al. [60] studied the comparative adsorption of Ni, Cu, and Zn by hydroxide and sulfide precipitation and reported more efficient removal by sulfide. A 95.32% Ni removal was achieved using sulfide precipitation compared to 76.66% hydroxide precipitation removal. In another study, Li et al. [58] removed Ti ions to trace levels through combining Fenton process and sulfide precipitation. The Fenton process achieved an excess of 95% Ti ion removal, and the sulfide precipitation made the method further effective to bring the ion concentration to trace levels in industrial wastewater.

3.1.2. Biological Precipitation. Metal ions can be precipitated as a consequence of the metabolism of microorganisms either directly or indirectly when they produce metabolites that react with the metal ions to precipitate them. Biological precipitation has been reported to offer better selectivity in metal ion removal compared to chemical precipitation. For example, the metal precipitation of engineered systems is optimized according to the rate of biological sulfide production, the precipitation of metal sulfides, and the quality of the metal precipitate product. In addition, it is low cost, applicable in low-metal concentration leachates, and it provides better settling. It is however more complex to operate compared to the chemical precipitation method [61].

Sulfate reduction by bacteria is a common method applied in heavy metal precipitation in this genre. A carbon source such as acetate, hydrogen, or sulfate is utilized to produce a sulfide under anaerobic conditions, which reacts with a metal ion to form a precipitable metal sulfide [62]. This method has been applied in metal recovery from an acid mine drainage system [63]. The [54] mechanism is illustrated in the following equations:

$$e^- \text{ donor} + S0_4^{2-} \longrightarrow S^{2-} + HCO_3^- \quad (1)$$

$$S^{2-} + Me^{2+} \longrightarrow MeS_{\downarrow} + H^+ \quad (2)$$

where e^- is an electron, Me^{2+} is a metal ion, and $MeS_{\downarrow}$ is the precipitated metal sulfide. In (1), sulfate-reducing bacteria act on the electron donor species, such as acetate, in a process to reduce the sulfate ions to sulfide ions. Organic compounds acting as electron donors are reduced to carbonates. In (2), the sulfide ion reacts chemically with dissolved heavy metal ions to produce precipitable metal sulfides that can be removed from the wastewater [62]. The process in (2) lowers the pH of the reaction medium due to the generation of high concentration of hydrogen ions. The acidity is neutralized through biogenic alkalinity resulting from equation (1). This is illustrated in equation (3) [64].

$$HCO_3^- + H^+ \longrightarrow CO_2(g) + H_2O \quad (3)$$

Another approach used in metal ion removal in biological precipitation is bioreductive precipitation, whereby the microorganisms utilize the metal ions in microbial metabolism. In this manner, metal-reducing bacteria take part in reducing the dissolved metal ions to precipitate. For example, uranium-reducing bacteria have been used in bioreducing uranium (VI) to uranium (IV) [65]. Some of these bacteria include denitrifiers, thermophilic bacteria, hyper thermophilic archaea, acid-tolerant bacteria, fermentative bacteria, and myxobacteria [64]. Some microorganisms are able to produce energy through bioreduction mechanisms by utilizing the metal as an alternative electron acceptor, while others reduce heavy metal cometabolically, in which case energy is not generated [66]. Growth of *Desulfotomaculum, Shewanella,* and *Geobacter* has been documented to increase with reduction of U6+ U4+, whereas *Desulfovibrio* shows cometabolic reduction when reducing U^{6+} [67]. Zhou et al. [68] used a hydrogen-based membrane in the removal of U^{6+} using a culture of *Desulfovibrio vulgaris* in which a sole electron acceptor of U^{6+} was fed. It was observed that the reactor performance increased to about 98% and then an almost complete reduction of U^{6+} occurred. Nanocrystalline UO_2 and U aggregates and precipitates were observed; authors associated them with vegetative cells.

3.2. Ion Exchange. This method is used mainly due to its major advantages in high efficiency and fast kinetics of heavy metal removal [69]. Ion exchange resins, which can either be natural or synthetic, are employed in this method. Synthetic resins are preferable due to their high efficiency [70]. The following equations show an illustration of ion exchange resin with the sulfonic acid group and a carboxylic acid group:

$$nR - SO_3H + M^{n+} \longrightarrow (R - SO_3^-)_n M^{n+} + nH^+ \quad (4)$$

$$nR - COOH + M^{n+} \longrightarrow (R - COO^-)_n M^{n+} + nH^+ \quad (5)$$

In (3), the exchange resin based on sulfonic acid group can remove metal ion by exchanging the hydrogen ion on the sulfonic group. In equation (4), the exchange resin is based on carboxylic acid. In a scenario similar to equation (3), the hydrogen ion on the carboxylic group is exchangeable for the metal ion.

Alyuz and Veli [70] studied the kinetics of the removal of nickel and zinc, based on ionic exchange resins, and found that ion exchange was highly dependent on pH, temperature, contact time, and initial temperature of the solution, whereby the major removal was acquired in the pH range of 4–6 for zinc and nickel ions. Abo-Farha et al. [71] observed similar results with cerium, iron, and lead ions and concluded that the adsorption sequence was $Ce^{4+} > Fe^{3+} > Pb^{2+}$.

3.3. Adsorption. The adsorption process is considered a thermal process that can occur physically or chemically. The adsorbate must adsorb to the pores of the adsorbent to be separated from the matrix through physical (physisorption) or chemical (chemisorption) processes [72]. During physisorption, van der Waals forces are the major players in the separation, while in chemisorption, separation relies on chemical interaction between the adsorbent and the adsorbate. Adsorbents fall under the following three classifications based on pore size: 2–5 nm pore sizes make up micropores, 5–50 nm make up mesopores, and 50–100 nm make up macropores [72]. This method of water purification is considered highly effective and economic since in many instances it results in highly purified effluents, in addition to being flexible in terms of design and operation [69].

Activated carbon is a commonly used adsorbent because of its high porosity; non-polarity; and made from carbon-rich materials of mineral, plant, or animal origin. The activation process can either be physical or chemical depending on the raw material and required texture. Physical activation mainly involves carbonizing the starting materials to about 450°C and then heating in carbon dioxide, air, or steam at temperatures of about 900°C at low pressures [72]. The porosity of activated charcoal can be as high as 2000 g/m^3, making it very useful for the removal of inorganic, organic, and biological waste in water [73]. However, its nonpolarity makes it a poor remover of heavy metals. To remove heavy metals from water, activated charcoal has to be modified chemically by the use of chelating groups [74]. Activated charcoal comes in either granular activated charcoal form or powdered activated charcoal form.

Carbon nanotubes (CNT) are carbon-based tubular structures entirely made up of hexagonally arranged hybrid carbon atoms [75]. They can be single-walled if made up of a singular sheet of graphene or multi-walled if multiple layers of graphene make up the structure [76]. CNTs attract attention as adsorbents as a result of their inert surfaces and

high specific surface areas, making them excellent physical adsorbers. They have been of great interest due to well-defined and uniform atomic structure compared to activated carbons [75]. Alijani and Shariatinia [77] fabricated a single-walled CNT-based nanocomposite for the removal of mercury from wastewater and achieved 99.56% adsorption in about 7 minutes. Single-walled CNT alone was reported to achieve about 45.39% adsorption of mercury.

A summary of the removal efficiency and operational cost estimates of some of the methods discussed is summarized in Table 2 [84].

4. Adsorbents

According to Pandit et al. [85], adsorbents can be defined as solid materials that can remove or separate contaminants from liquids or gases to avoid environmental harm. The separation of contaminants is usually based on their selective binding, or adsorption, on the surface of the adsorbent. This selectivity can be kinetic and/or thermodynamic, based on the specific interaction between the adsorbent's surface and the contaminants. In this manner, there's an underlying complex interaction among these three components, namely the adsorbent, adsorbate, and wastewater [86]. The relationship is illustrated in Figure 2 [86].

In the ternary system illustrated in Figure 2, the main interaction that controls the entire adsorption system is between the adsorbate and the adsorbent. Other factors, however, come into play to affect this interaction, that is the affinity between the solution and the adsorbate, solution and the adsorbent, and the contaminants. Owing to low solubility, hydrophobic compounds in aqueous solutions are observed to get attracted to the surface of the adsorbent. Therefore, the adsorption capacity is considerably dependent on the forces that arise from the interaction of these three components [86]. Since the adsorption is by principle a surface phenomenon, any solid needs to be porous and possess a large surface area, to be considered an adsorbent. In addition, other considerations are based on: ready availability and low cost, great physical strength especially in solutions, good mechanical properties, ability to regenerate, and long life [87].

In order to ensure efficient contact between the adsorbent and the wastewater, different systems have been proposed and applied both at the industrial and laboratory level. Some of these methods include mobile mat filters, pulsed beds, fluidized beds, fixed bed-type processes, and batch methods. Depending on the application, the most common systems are fixed bed and batch-type processes. When a continuous system for contact is necessary, like in an industrial scale, the fixed bed-type contact system (reactor and columns) is applicable, while for laboratory-level experimentation, batch processes are usually applicable [88]. The batch processes are necessitated at laboratory scale due to their efficiency at small volumes of wastewater, ease of use, and simplicity.

In fixed bed reactors, adsorption is heavily dependent on the concentration of the adsorbate in the wastewater. The contaminated solution (wastewater) is always in contact with the adsorbate, which with continuous adsorption of the solute ensures continuous dynamism in the concentration of the adsorbate in the solution. This system offers great mass and heat transfer and greater residence times than any other batch reactor on the industrial scale [88]. Mat filters are often implemented as depth filters with the ability to separate contaminants from the liquid phase through sieving, interception, and adsorption [89]. They are referred to as depth filters because they not only filter on the surface but also in the interior pores through adsorption [90]. Due to the intimate contact, they introduce between the adsorbate and adsorbent in the liquid phase, they are most applicable when the influent contains high particulate matter [91]. Yigzaw et al. [90] and Shukla and Kandula [91] have utilized mat filters in biological sciences for antibody purification and recovery. For application in wastewater treatment, nanofibers have been used in mat filter fabrication to adsorb various heavy metals such as Cu^{2+} and Pb^{2+} [92].

In pulsed bed adsorption, the feed flows from the underside of the adsorbent material upwards. When the adsorbent is spent, it is removed from the bottom and refilled from the top (i.e., opposite the flow of the feed) to ensure a constant column height to maintain efficiency [93]. Pulsed bed adsorption is most preferable when the adsorbent and the feed are of a high relative performance rate. Fluidized beds are incorporated when high heat and mass transfer applications are required. Most sets incorporate adsorption and desorption sections to improve the efficiency of the process. During adsorption, a solid adsorbent is fluidized by the upward movement of the mobile phase influent, causing a downward "flow" of the adsorbent as a fluid. This increases contact between the phases and thus high adsorption is possible in this setup. The fluidized adsorbent falls to a lower desorption bed whereby desorption occurs through heat exchange and the adsorbent can be gased to the top of the column for cycling [94].

In an effort to control the liquid-phase adsorption performance in a solid material, a number of factors affect the adsorption process. Some of these factors include ([95] (1)) the nature and origin of the adsorbent solid. This includes the physical considerations such as the specific surface area, the particle size, and porosity; chemical considerations including the functional groups of the solid, surface charge, and pH when the solid has no charge; and mechanical properties. (2) Conditions necessary for the activation of the solid. These include considerations such as chemical or physical treatment to activate the material and the effects of the variables of the process applicable in the contacting system. These variables include the initial concentration of the pollutants, contact time, stirring rate, and solid dosage. (3) The mechanism of removal of the pollutants. This includes the conditions of the solution such as the temperature, pH, presence of impurities, among others.

Adsorbents have been classified to five categories according to Crini et al. [86]. This classification is based on the applications of the adsorbent in both the industrial setting and the applicability in laboratory practice. Natural materials are adsorbents that include wood, bauxite, sawdust, and fuller's earth. Treated natural materials are another classification that

Table 2: Removal efficiency and removal cost estimate of various methods.

Method	Operational cost estimate per year (USD)	Removal efficiency		References
		Contaminant	Removal capacity (mg/g or%)	
Reverse osmosis	~17 million	Cu^{2+}	98%	[78]
		Cd^{2+}	99%	
		Pb^{2+}	99%	[79]
		Zn^{2+}	97%	
Nanofiltration	~17 million	Cu^{2+}	>90%	[80]
		As^{3+}	48%	
Ion exchange	3 million	Hg^{2+}	99.9%	[81]
		Ni^{2+}	99.9%	
Electrodialysis	150, 000	Fe^{2+}	>66%	[82]
		Ag^{+}	99%	
Granular activated carbon	74–209 million	Pb^{2+}	16.2 mg/g	[83]
		Cr^{3+}	638 mg/g	

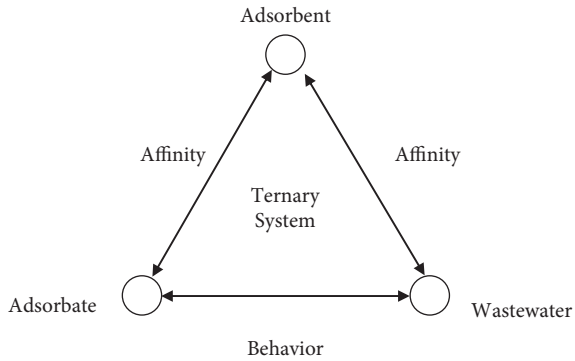

Figure 2: Relationships of a three-component adsorption system.

include activated carbons, silica gel, or alumina. Manufactured materials such as zeolites, resins, and aluminosilicates are also among the adsorbent classification. Another type is the industrial by-products and solid agricultural wastes such as red mud and fly ash. The last type is the biosorbents that include fungi, chitosan, cellulose, among others.

4.1. Low-Cost Adsorbents. Agricultural wastes and biosorbents are termed low-cost adsorbents due to their abundant nature and they inexpensive and potential to act as complexing materials [95]. Chitosan occurs naturally in large amounts and is a low-cost sustainable adsorbent for waste water remediation [96]. It has been reported to bind effectively with small ionic diameter metal ions such as Cu (II) ions. To effectively remove larger ions, chitosan has been modified to improve its structural properties [96]. Hosseinzadeh and Ramin [97] used a magnetic chitosan/graphene oxide nanocomposite to remove copper ions from wastewater and reported a maximum adsorption capacity of approximately 217.4 mg/g.

Cellulose is one of the most abundant biopolymers that are biodegradable, insoluble in most solvents, and non-meltable [98]. The most common commercial sources of this abundant material are wood and cotton but it is extractable from other credible sources. Cellulose exhibits low adsorption in an unmodified state and to be utilized for heavy metal adsorption as a low-cost adsorbent, it often requires modification [98]. Dridi-Dhaouadi et al. [99] investigated the adsorption of lead (II) ion and yellow 44 dye by unmodified cellulose isolated from *Posidonia oceanica* and observed that the cellulose had higher adsorption for lead than for dye. Wu et al. [100] also investigated the adsorption of lead (II) ions on cellulose and reported optimum removal at a pH of 6 with a maximum adsorption capacity of 10.78 m^2/g. The authors also reported that modification of the cellulose with thiol groups increased metal adsorption.

5. Clay

5.1. Structure and Properties. aClay essentially refers to soil particles of the size less than 5 μm or rock made up of clay minerals. Clay exhibits high plasticity when wet, and is considered coherent when dry [101]. In soil, it ensures proper porosity; good water retention; and acts as a reservoir for nitrogen, calcium oxide, and potassium oxide minerals [102]. Clay minerals are produced majorly through weathering, hydrothermal alteration, and diagenesis processes [102]. Clay minerals are structured to magnesia or alumina octahedral sheets and silica tetrahedral sheets (Figure 3). According to the arrangement of these sheets, clay minerals are classified into four main groups namely kaolinite, chlorite, illite, and smectite [103] and are shown in Figure 3 [104].

In kaolinite, the structure arrangement between the octahedral and tetrahedral sheets is in a ratio 1 : 1 and consists of kaolinite, halloysite, dickite, and anauxite. The charges between the two layers are usually balanced, and thus the clay does not swell. The chlorite group includes an extra brucite layer alternating with tetrahedral-octahedral-tetrahedral layers [105]. The illite and smectite form tetrahedral-octahedral-tetrahedral layers (i.e., 2 : 1 ratio) joined to each other by hydrogen bonding and electrostatic forces [103]. The smectite group, consisting of bentonite and montmorillonite (MMT), exhibits a higher swelling capacity than illite. For application in heavy metal removal, the clay

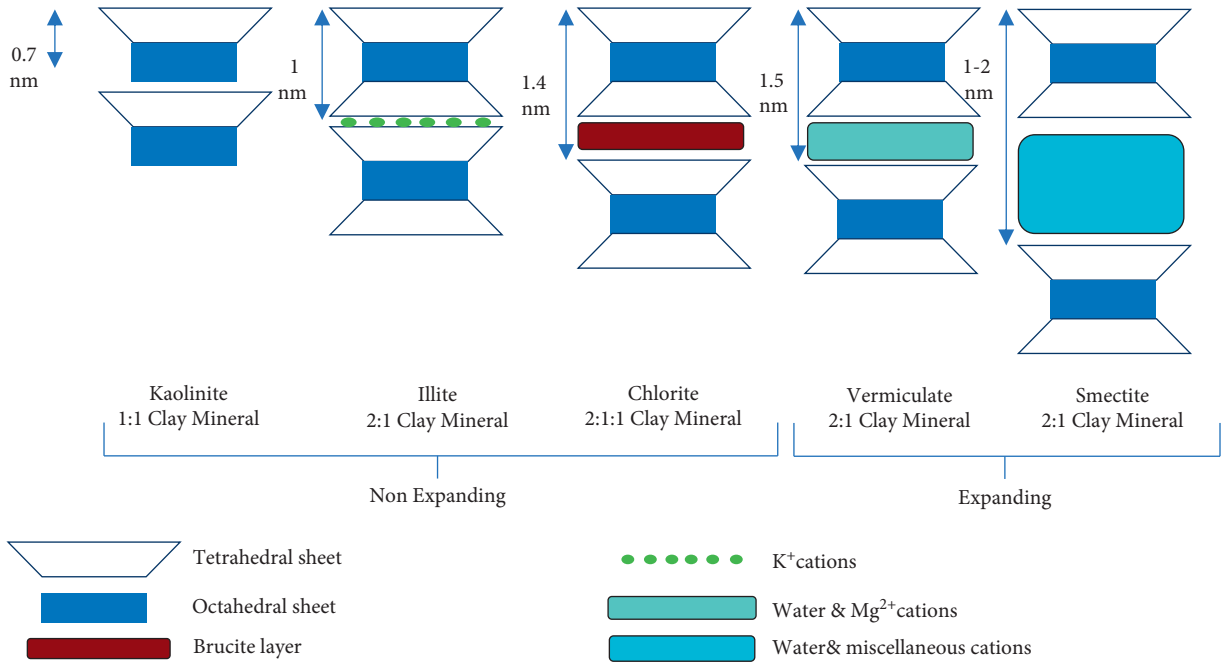

Figure 3: Classes of clays according to structural arrangement (Ghadiri et al., 2015).

mineral needs to have a high cation exchange capacity (CEC) and a specific surface area. CEC is a characteristic quality of soil to hold positively charged ions [106]. Karpiński and Szkodo [105] reported that the smectite group has a higher CEC (80–150 meq/100 g) and a specific surface area (800 m^2/g) compared to illite (10–40 meq/100 g, 15 m^2/g). Kaolinite was reported to have the lowest CEC.

Clay on its own has been applied in heavy metal removal by various researchers. Kaolinite in raw and modified forms has been used in the removal of chromium (VI) ions, and adsorption has been reported to be highly sensitive to the pH of the solution, with increasing adsorption from pH 1 to 7 [107]. Montmorillonite clay has also been used in the removal of lead (II) ions in its raw form and maximum adsorption is reported to be about 28 mg/g [108]. In modified form, montmorillonite was reported to increase metal ion adsorption to 131.579 mg/g owing to an increase in active sites with modification by acetic acid [109]. Bentonite has been applied in the removal of various heavy metal ions including copper (II), cobalt (II), nickel (II), and lead (II). The highest adsorption capacity of lead (II) by unmodified bentonite is 59.7 mg/g and in modified form is 123.3 mg/g [24]. Al-Jlil [110] reported that the maximum removal of chromium (III) by raw bentonite was 13.79 mg/g and in a modified state of 4-*aminoantipyrine*, the adsorption capacity was 38.8 mg/g.

5.2. Types of Nano-Clay-Based Adsorbents. Clay is employed as a nano adsorbent in several adsorption procedures due to its unique characteristics and high removal effectiveness [111]. Nanoclays are a potential property enhancer that has been discovered to be super effective in the purification of water. A large number of researchers have investigated the use of clay minerals as adsorbent materials for the adsorption of different hazardous substances such as heavy metals, coloring agents, antibiotics, biocide substances, and other organic chemicals. Nano adsorbents are made up of nanoparticles with a large specific surface area and connected sorption sites. The sorbent exhibits better adsorption for organic chemicals due to the short intra-particle dispersal distance and adjustable pore size and surface chemistry.

5.2.1. 1D Clay Nano Rods. Attapulgite (APT) is a one-dimensional (1D) clay that is natural with a structure comparable to carbon nanorods. Awasthi et al. [112] suggest that the APT is made up of 2 : 1 phyllosilicate ribbons, with interspaces between them measuring around 0.4 nm × 0.6 nm. Natural APT has a good adsorption capacity for dyes and heavy metals, thanks to these zeolite-like nano channels. Because of the hydrogen bonds and Van der Waals force, natural APT exists as mass aggregated crystal bundles that inhibit dye macromolecules from reaching efficient interaction with sites that are active sorption. The fabrication of 1D APT nanorods by shattering bulk bundles has sparked a lot of curiosity lately. The permanent inherent negatively charged electrode and specifically large surface area of disintegrating 1D APT nanorods enabled the development of adsorbents that were 1D APT based.

They can develop hybrids with materials that are 2D layered depending on different 1D morphology of APT nanorods to acquire the highly customizable framework for making full use of the properties of nanorods and nanosheets. Clay/APT nanocomposites were made by mixing 1D APT with 2D bentonite nanosheets using homogenization of a high-pressure. When APT was added, the rate of hydration of bentonite and salt resistance improved, resulting in a higher dosage of MB adsorbent in the presence of sodium chloride. [113] developed a ceramic-supported composite film of attapulgite/graphene oxide (GOA) with 1D APT

inserted into 2D lamellar GO sheets, allowing high-flux water transport through nano channels. The prepared GOA showed about 100% disapproval efficacy against Ni^{2+}, Cd^{2+}, Pb^{2+}, and Cu^{2+}. This was due to the size exception effect, that was based on nanotube correlation between the GO layers formed by 6 APT nanorods.

5.2.2. 2D Clay Nanosheets. Clay minerals are mostly made up of 2D nanosheet units, which are made up of a set of neatly stacked layers [114]. Strong interactions such as hydrogen bonding combine neighboring 2D nanosheet units, while Van der Waals weak forces combine adjacent 2D nanosheet units. Such clays have strong adsorption capability due to the unique interlayer space, that has been extensively used in the pollutant removal from wastewater. However, because the various sites of adsorption on the interior surface have not yet been fully explored, the effectiveness of lamellar clay as an adsorbent is diminishing when used immediately. Exfoliated 2D clay nanosheets were able to totally release active adsorption sites and considerably increase the surface area, both of which are beneficial to improving adsorption performance. Because of its good hydration swelling property, montmorillonite clay can be easily exfoliated into 2D nanosheets. The fabrication of a range of sophisticated functional nanocomposites using 2D MMT nanosheets (MMTNS) with completely visible sites that are active following exfoliation has further pushed the use of MMT as adsorbents. According to El Kassimi et al. [114], the hydrogel phase with three-dimensional macroscopic nanostructures is particularly helpful for simple solid-liquid separation succeeding in removing contaminants from liquids, among the many MMTNS-based adsorbent materials. Also, the hydrogel's ion diffusion velocity is comparable to that of water, resulting in faster adsorption kinetics. As a result, hydrogels are becoming an interesting topic in search of adsorbents that are novel and can effectively remove pollutants from water.

El Haouti et al. [115] created a new self-assembled gel for the removal of MB under the influence of H_2O_2 under visible light. The Fe-CS/MMTNS gel with iron demonstrated outstanding reuse and maintaining quality MB removal efficiency attributed to the synergistic impact of reaction of Fenton and adsorption degradation. Due to the complex formation between iron and chitosan, the Fe-CS/MMTNS is stable and operates well across a wide pH range attributed to the prevalence of hydroxyls on the surface of MMTNS (CS).

5.2.3. Clay-Supported Nanoparticles as Composites. Nanoparticles (NPs) are a form of adsorbent that uses nanoscale effect, extremely high surface area, and reactivity to remove contaminants from water. NPs are tiny atomic clusters that are less than 100 nanometers in size. Although NPs have a larger capacity of adsorption than micron-sized counterparts because of their nano size-particle distribution, NPs are more afflicted to clustering in water because of their increased energy of the surface, which reduces effective sorption. As a result, the main hurdles in the use of nano adsorbents are ensuring NP disposability after adsorption in liquid/solid dissociation and water. Masoudi et al. [116] developed nanoscale Fe_2O_3-treated halloysite nanotube (HNT) adsorbents for treating excess phosphate in water and preventing eutrophication. The surface charge density of treated iron oxide was observed to boost the capacity of adsorption of the nano adsorbent toward phosphate. To remove dyes, Rafati et al. [117] used a carboxymethylcellulose-bentonite (LCB) composite loaded with lanthanum (La). By crosslinking clay and polymer, the addition of La^{3+} strengthened the framework. In the field of geo-engineering, Phoslock®, a type of lanthanum (La)-modified bentonite clay, has been utilized to regulate oxyanions in waste streams and sediments.

5.2.4. 1D Clay Nanotubes. Halloysite nanotubes (HNTs) represent one-dimensional tubular clay. Such naturally present nano-minerals are gaining favor as low-cost options to produced nanotube substances like carbon nanotubes, thanks to the exceptional properties of a 1D tubular structure. Shapira and Zucker [118] created an Ag_3PO_4-HNT adsorbent for the treatment of polluted water. The adsorbent produced was capable of adsorbing soluble dyes and medicinal compounds on HNT, which were subsequently photocatalyzed by Ag_3PO_4 and destroyed in visible light. Zhang et al. [111] created a redox-participating HNT-CeOx($x = 1.5$–2.0) nanohybrid. Electrostatic interaction uniformly coated CeO_2 nanoparticles on the HNT substrate, greatly increasing the adsorption capacity of As (III) (209 mg/g) compared to unsupported CeO_2 nanoparticles (62 mg/g).

5.3. Clay-Based Nanocomposites as Adsorbents. Nanocomposites have been reported to possess high porosity and immense surface area making them excellent candidates for heavy metal removal [24]. The most important properties for good adsorption (porosity, active surface area, CEC, pore volume among others) are enhanced by one or more components of the nanocomposite [24]. Clay polymer-based nanocomposite adsorbents such as cellulose-montmorillonite [119], polyaniline-montmorillonite [120], poly (acrylic acid)/organo-montmorillonite [121], and β-cyclodextrin based bentonite [122] have been reported.

Irani et al. [123] synthesized an organomontmorillonite hydrogel nanocomposite for the removal of lead (II) ions and reported a maximum removal capacity of 430 mg/g. Other researchers have also reported lead (II) ion removal by use of clay-based nanocomposites [124, 125]. On the chitosan-clay nanocomposite, the maximum adsorption of cadmium (II) ions was reported to be approximately 72.31 mg/g by Tirtom et al. [126]. The maximum adsorption of chromium (III) ions was reported to be about 0.25 mg/g on a similar chitosan-clay nanocomposite [127].

Copper (II) ion removal has previously been investigated by the use of various nanocomposites [125, 128–130] and the maximum adsorption reported to be about 106.2 mg/g when polyacrylamide-bentonite (PAA-B) nanocomposite modified with humic acid-immobilized-amine [128]. In a different study, the adsorption capacity was observed to increase from 11 mg/g to 20 mg/g in PAA-B when the pH of the solution was reduced from 6.2 to 5 [131].

Removal of nickel (II) ion has also been studied and reported by various researchers [126, 132–134]. Tirtom et al. utilized an epichlorohydrin crosslinker in chitosan-clay nanocomposite in a study to comparatively adsorb nickel (II) and cadmium (II) ions. According to the Langmuir isotherm, Ni^{2+} removal was reported to be 32.36 mg/g and 72.31 mg/g for Cd^{2+}. Zhang and Wang [134] used a low-cost lignocellulose/montmorillonite nanocomposite to adsorb nickel (II) ions from synthetic wastewater. At a solution temperature of 70°C and a pH of 6.8, the ion's adsorption was reported to reach 94.86 mg/g. García-Padilla et al. [132] reported high nickel (II) adsorption (97.1%) at a pH of 4.5 using starch/sodium montmorillonite nanocomposite.

Other reports are summarized in Table 3.

6. Adsorption Studies

6.1. Factors Affecting Adsorption. For a fixed amount of the adsorbent, an optimum concentration of the ion to be removed is required. When the initial ion concentration is low, adsorption tends to be slow. Increasing the initial ion concentration increases the adsorption rate, up to a certain point, beyond which removal decreases. This is attributed to the flooding of metal ions for an unchanging number of adsorption sites [139]. In agreement with this, Hassana and Shaban [140] reported that Fe^{3+} adsorption onto kaolinite increased with an increase in initial metal ion concentration. Sallam et al. [141] in a study to remove Cr^{6+} ions from tannery wastewater reported the highest removal ranging from 76.3% to 100% occurring with initial metal ion concentrations ranging from 10 to 50 mg/L. This illustrated that metal ion removal occurred best with relatively high initial concentrations.

At low pH, hydrogen ions are abundant in the solution, and thus they compete with metal ions for active sites on the adsorbent, thus lowering the adsorption of heavy metal ions. Research conducted by [142] to investigate the effect of pH on Hg (II) found that an increase of pH from 2 to 5 had increasing Hg adsorption. Similar studies on the removal of lead and copper by Razzaz et al. [92]found more removal at pH 6 and least at pH 2 to 4. Zhao et al. [131] studied the removal of Cu^{2+} ions using bentonite-polyacrylamide composite and reported a massive removal increase from 9% to 97% as pH was increased from 2 to 7. Cadmium removal maxed out at pH 9 in a study conducted by Kim et al. [143], achieving adsorption of 97%. Studies by Ravikumar and Udayakumar [144] also agree to this phenomenon for the removal of Cd^{2+} and Pb^{2+} achieving maximum metal ion removal at a pH of 6 for both of them, using *Moringa oleifera*/montmorillonite nanocomposite. Beyond this pH, the metal ions seemed to precipitate. In the same study, Cr^{6+} ion adsorption disagreed with this phenomenon and showed high adsorption at low pH values of 2 and 3. This was because the ions in solution existed as polyanions of $HCrO_4^-$, CrO_4^{2-}, and $Cr_2O_7^{2-}$ at low pH. Xu et al. [145] agreed with this in a similar investigation.

Concerning contact time, heavy metal ions in contact with the nano adsorbent enhance the adsorption. At the initial stage, adsorption will occur quickly because of the abundance of active sites and later slow down to a point where the adsorption is independent of the contact time. At this point, the system has reached an equilibrium between the adsorption and desorption processes [139]. A study by Jiang et al. [146] on heavy metal adsorption by kaolinite clay reported high initial heavy metal ion removal within the first 30 minutes that gradually achieved equilibrium. It was also observed that the rate of removal was ion dependent with percentage removal represented as Pb (II) > Ni (II) > Cd (II) > Cu (II) ranging from highest removal to lowest. Masheane et al. [147]used a chitosan-based nanocomposite to remove chromium and nitrate ions and reported rapid ion removal in the first 30 minutes of application. The activity was insignificant by the 60^{th} minute which translated to a rapid saturation of active sites of adsorption on the nanocomposite material.

Temperature initially affects the viscosity of the solution, enhancing the diffusion rates of the heavy metal ions. An increased temperature can affect the adsorption process depending on whether the mechanism is exothermic or endothermic. In the case of exothermic adsorption, an increase in temperature will decrease the rate of adsorption due to the effect of heat on electrostatic interactions between the metal ions and the adsorbent in addition to desorption attributed to high ion mobility due to elevated temperatures [142]. In the case of endothermic adsorption, an increase in temperature enhances adsorption. This is attributed to increased ion mobility that results in greater access to active sites [148]. Murithi et al. [149] reported an increase in adsorption of cadmium (II) ions with an increase in temperature from 20°C to 43°C beyond which removal decreased, using the biomass of water hyacinth roots. This implied an endothermic adsorption process. Zhao et al. [131] reported Cu^{2+} adsorption increase with an increase in temperature of solution attributing it to a decrease in the ionic strength of the solution as the temperature rose.

6.2. Adsorption Isotherm Models. Isotherms describe the effect of concentration on metal ion adsorption at a constant temperature. The most common isotherm models used to describe adsorption isotherms are the Langmuir and Freundlich models [139]. Others are Temkin and Dubinin-Radushkevich, well discussed by Dada et al. [150].

Langmuir's model, depicted in the following equation [151], describes adsorption in the case of a monolayer surface with equivalence in the affinity of the adsorbate ions.

$$\frac{C_e}{q_e} = \frac{1}{Q_0 b} + \frac{C_0}{Q_0}, \tag{6}$$

where q_e represents the amount of metal ion adsorbed (mg/g), C_e is the equilibrium concentration (mg/L), Q_0 represents the adsorption capacity (mg/g) and b is the Langmuir's constant (L/mg). The slope and intercept of the plot of (C_e/q_e) to C_e give $1/Q_0$ and $1/Q_0 b$, respectively.

In the case of heterogeneous adsorption, whereby adsorbent surface texture matters, the Freundlich model is considered. It is represented by the following equation [152]:

Table 3: Previous reports on heavy metal removal by clay-based nanocomposites.

Clay-based nanocomposite	Polymer used	Metal removed	Adsorption capacity (mg/g or %)	Observations	Reference
2-Aminophenol and 2-nitrophenol/iron montmorillonite	2-Aminophenol and 2-nitrophenol	Fe (III) Fe (II)	29% (adsorption area) 71% (adsorption area)	At high ranges of pH, reduction occurred in the phenolic ring.	[135]
β-Cyclodextrin/bentonite	β-cyclodextrin	Cu (II) Zn (II) Co (II)	94% 98% 92%	Metal concentration was 20 mg/L	[122]
Ion-imprinted polymer/ diazonium montmorillonite	Cu (II) imprinted polymer	Cu (II)	23.3 mg/g	Adsorption capacity maxed out at pH 5.	[136]
Polyacrylamide/sodium montmorillonite nanocomposite	Polyacrylamide	Co (II) Ni (II)	98.67% 99.30	Highest removal of Ni (II) occurred at a pH of 7 and Co (II) at pH 6	[137]
Modified montmorillonite/ polyethersulfone-mixed matrix membrane	Polyethersulfone	Zn (II) Ni (II)	88.9% 74.4%	Highest removal was achieved with 3% clay mixture into the polymer matrix	[138]

$$\log q_e = \log K_f + \frac{1}{n}\log C_e, \tag{7}$$

where K_f and n represent Freundlich constants that correspond to heterogeneity and the bonding energy, respectively. These values arise from the intercept and slope of the plot of $\ln q_e$ to $\ln C_e$, respectively.

The Sip isotherm model exists to cross between the Freundlich and the Langmuir's isotherm models. It combines them through linear (8) [153]. A low concentration in this model describes adsorption in terms multilayer coverage, or Freundlich, while a high concentration describes adsorption in monolayer coverage, or Langmuir.

$$\frac{1}{q_e} = \frac{1}{Q_{\max}K_s}\left(\frac{1}{C_e}\right)^{(1/n)} + \frac{1}{Q_{\max}}, \tag{8}$$

where K_s, given in L/mg, is described as the adsorption affinity and n is the heterogeneity index. These two values are derived from plots of $(1/q_e)$ against $(1/C_e)^{(1/n)}$.

The Dubinin-Radushkevich (D-R) adsorption isotherm is modeled to describe adsorption in terms of porosity and free energy. Its major purpose is to differentiate the adsorption mechanisms as either physisorption or chemisorption. This model is described as follows [154]:

$$q_e = Q_{DR}\exp\left(-K_{DR}\left[RT\ln\left(1-\frac{1}{C_e}\right)\right]^2\right), \tag{9}$$

$$\ln(q_e) = \ln Q_{DR} - K_{DR}\left[RT\ln\left(1+\frac{1}{C_e}\right)\right]^2, \tag{10}$$

where q_e in mmol/g represents the amount of metal ions adsorbed at equilibrium. Q_{DR} in mmol/g describes the maximum adsorption capacity at equilibrium. K_{DR} in mol^2/kJ^2 is usually a constant referred to as the Dubinin-Radushkevich constant. C_e in mol/dm^3 is the quantity of the metal ion adsorbed at equilibrium. (9) and (10) describe only the porosity aspects of the model and therefore are not conclusive on their own. An additional (11), therefore, relates the K_{DR} value to free energy [155].

$$E = \frac{1}{\sqrt{2K_{DR}}}. \tag{11}$$

The values of E are useful for estimating the type of adsorption that occurs. When $E < 8$ Kj/mol, the adsorption is described as physisorption. When $E > 8$ kJ/mol, the adsorption process is described as chemisorption [153].

Temkim isotherm model has the implication that the heat of adsorption is describable linearly, rather than logarithmically. This model ignores the extremes of very high or low concentrations. Among other factors, consumption is also uniform in distribution of boundary energy up to certain limits described as maximum bonding energy [155]. This model is described by

$$q_e = B\ln A + B\ln C_e. \tag{12}$$

In addition to the common parameters in isotherm models, B introduced in the Temkim model is a constant that is relatable to the heat of adsorption by the following equation:

$$B = \frac{RT}{b}, \tag{13}$$

where b (J/mol) and A (L/g) are Temkim constants arising from slopes (B) and intercepts ($B\ln A$), respectively, of the plot of q_e versus $\ln C_e$ [155].

Sharma et al. [156]studied adsorption isotherms using both Langmuir and Freundlich model at a pH of 6 and a temperature of 25°C for a period of 2 hours. The authors reported the adsorption to be best described by the Freundlich model owing to the highest correlation coefficient values for all the studied heavy metal ions (Pb^{2+} and Cd^{2+}). Sallam et al. [141] used Langmuir, Freundlich, and Temkim isotherm models for adsorption of Cr^{6+} and reported that the adsorption was best described by the Freundlich model. This meant that the ion adsorbed onto

heterogeneous areas using different binding energies. Additional literature is summarized in Table 2.

6.3. Adsorption Kinetics. Adsorption kinetics tries to describe the adsorption based on time and metal ion concentration. Various models have been used to describe adsorption kinetics, among which are pseudo first- and second-order, double exponential, and intra-particle diffusion [139].

Pseudo first-order is described as follows [136]:

$$\log(q_e - q_t) = \log q_e - \frac{k_1}{2.303}t. \quad (14)$$

The integrated rate of pseudo second-order equation is illustrated as follows [141]:

$$\frac{t}{q_t} = \frac{1}{k_2 q_e^2} + \frac{t}{q_e}. \quad (15)$$

In (5) and (6), q_t represents adsorption capacity, at time, t. q_e represents adsorption at equilibrium, given in mg/g. k_1 and k_2 are pseudo first-order and second-order rate constants, respectively, given in min^{-1}. T is the contact time in min. The intercept and slope of $\log(q_e - q_t)$ versus t for pseudo first-order gives the q_e and k_1 values, respectively. In the case of pseudo second-order, the intercept and slope of the plot of (t/q_t) versus t gives k_2 and q_e (equilibrium adsorption capacity), respectively.

The intra-particle diffusion model describes the adsorption of ions from the solution to the surface of the adsorbate and diffusion into the interior of the pores. It is represented in (15) [157].

$$q_t = K_{id}t^{0.5} + C, \quad (16)$$

where q_t represents the adsorption capacity at time, t. $t^{0.5}$ represents the half-life time given in seconds. K_{id} represents intra-particle diffusion rate constant in $\text{m/g}\cdot\text{min}^{0.5}$. The boundary thickness is represented by C. The values of C and K_{id} are given by the intercept and slope of the plot of q_t versus $t^{0.5}$.

Previously reported adsorption parameters are summarized in Table 4.

Sharma et al. [156] used pseudo 1st order, pseudo 2nd order, and intra-particle diffusion to study the adsorption kinetics of mesoporous ZnO and TiO_2@ZnO monoliths and reported the adsorption kinetics best fitted the pseudo second-order kinetics. This translated to the fact that the adsorption mechanism of the metal ions was mostly chemisorption. Sallam et al. [141] used many kinetic models to study Cr^{6+} adsorption and reported that the adsorption kinetics best fit the pseudo second-order model with a very high correlation coefficient. This meant that the adsorption was most likely based on chemisorption mechanism.

6.4. Thermodynamics of Adsorption. Thermodynamically, adsorption can be described as either endothermic or exothermic. An increase in adsorption with an increase in temperature presents an endothermic process, while a decrease in adsorption with increasing temperature describes exothermic adsorption [163].

Adsorption thermodynamics behavior can be determined using Gibb's energy, enthalpy, and entropy [164].

$$K_d = \frac{C_A}{C_B},$$

$$\Delta G^0 = -RT \ln K_d, \quad (17)$$

$$\ln K_d = \frac{\Delta S^0}{R} - \frac{\Delta H^0}{RT},$$

where K_d represents thermodynamic equilibrium constant, T is the absolute temperature in Kelvin, R universal gas constant, C_A and C_B the concentration of the adsorbate on the adsorbent and residual concentration at equilibrium, respectively [163].

A negative ΔH^0 represents an endothermic adsorption process, while a positive value represents exothermic adsorption. Negative ΔG^0 hints at spontaneous adsorption, which interprets that the adsorption is possible at any temperature. A negative ΔS^0 hints at low randomness at adsorption [163].

Sharma et al. [156] reported the adsorption of Pb^{2+} and Cd^{2+} ions on ZnO and TiO_2@ZnO monoliths to be endothermic and spontaneous in respect to a negative Gibb's energy and a positive enthalpy. They also reported positive values of entropy due change of energy between the monoliths and the metal ions adsorbed. Other reports on thermodynamic adsorption parameters are summarized in Table 5.

7. Analytical Techniques

7.1. Scanning Electron Microscopy and Transmitted Electron Microscopy. Scanning electron microscopy (SEM) and transmission electron microscopy (TEM) are extremely essential techniques to understand the surface, morphological, and chemical interactions of materials. Both methods work differently, but the common feature between them is an electron lamp, electron apertures, and electromagnetic lenses.

SEM scans the samples in a raster fashion, detecting backscattered electrons and reflected electrons to give data about the surface of the material. It is limited to a scan area of 0~5 nm. The sample needs to be positioned at the end of the apparatus for quality scanning. TEM functions by detecting the electrons that pass through (transmit) the sample. Due to the nature of the electron, the samples need to be very thin, typically less than 150 nm. For the SEM analysis of clay-cellulose nanocomposite, clay particles are expected to be coarsely aggregated in the matrix. Mirsafaei and Kolahdoozan [167] analyzed the morphology of the poly (amide-ester-imide)/sodic montmorillonite nanocomposite using SEM and observed polymer particles inserted "crystallographically regular" in the clay structure.

Table 4: Previously reported adsorption parameters of clay polymer adsorbents.

Adsorbent	Metal ion	Modifying agent	Optimum parameter	Adsorption capacity (mg/g)	Isotherm	Kinetic model	References
Poly (acrylic acid)/ attapulgite nanocomposite	Pb (II)	Acrylic acid	pH = 5	38.0 mg/g	Freundlich	Pseudo 2^{nd} order	[158]
Bentonite cellulose nanocomposite	Cu (II)	L-cysteine	Temperature = 50°C	32.37 mg/g	Langmuir	Pseudo 2^{nd} order	[159]
Cysteine/ Montmorillonite nanocomposite	Pb (II)	Cysteine	—	0.180 mg/g	Freundlich	—	[160]
Sepiolite polymer nanocomposite	Cu (II)	Vinyltriethoxysilane	pH = 5.4	86%	—	Pseudo 2^{nd} order	[161]
Polyetherimide/grafted bentonite membrane	Pb (II) Cd (II)	Polyetherimide	Membrane porosity = 62.7% Water uptake = 71.3%	80% (Pb ion) 76% (Cd ion)	Langmuir	Pseudo 1^{st} order	[162]
Ion-imprinted clay/ polymer nanocomposite	Pb (II)	Visible light initiation	pH = 6.5	301 mg/g	Langmuir	Pseudo 2^{nd} order	[136]

Table 5: Thermodynamic parameter of various clay polymer-based heavy metal adsorbents.

Adsorbent	Adsorbate	T (K)	ΔG^{o} (kJ/mol)	ΔH^{o} (kJ/mol)	ΔS^{o} (J/mol/K)	References
Polyacrylamide/bentonite hydrogel nanocomposite	Pb (II)	303	−5.81	1.42	20	[165]
		313	−6.02			
		323	−6.29			
	Cd (II)	303	−5.11	9.34	40	
		313	−5.58			
		323	−6.06			
Cellulose-montmorillonite nanocomposite	Cr (III)	298	−3.434	90.07	313.02	[119]
		308	−6.455			
		318	−9.685			
Cellulose-montmorillonite nanocomposite	Cu (II)	293	−6.796	−40.456	−116.81	[166]
		303	−4.308			
		313	−3.794			
		323	−2.356			
	Cd (II)	293	−2.041	−29.639	−86.216	
		303	−5.243			
		313	−2.243			
		323	−2.145			
		333	−2.794			

SEM data are important in the analysis of surface characteristics of materials [168]. Data arising from TEM are important in detecting the internal workings of a sample inclusive of crystal structure, morphology, and stress state. TEM has been reported to achieve extremely low optical spatial resolutions of less than 50 pm [169].

Sallam et al. [141] used SEM technology to characterize a polymer-clay nanocomposite and reported smooth surfaced sticking particles that were associated with the polymerization process. The authors used XRD and FTIR techniques to describe further characteristics of the material. Khan et al. [170] used TEM to observe the structure of polyacrylamide/bentonite hydrogel nanocomposite. The authors reported complete random exfoliation of the bentonite particles. This was so because ultrasonic synthesis was applied during the fabrication of the nanocomposite. The SEM data from the same researchers for the raw and nanosized bentonite clay had rougher texture compared to the hydrogel nanocomposite, which showed uniform texture on the surface which did not agglomerate. Other reports on SEM and TEM analysis have been summarized in Table 6.

7.2. X-Ray Diffraction. X-ray diffraction (XRD) was developed to characterize materials by analyzing the crystalline structure of the material [175]. The principle of operation is that when a high-energy electron beam displaces an electron from the inner shell of an atom, the outer shell electron cascades to fill the gap left releasing energy in the form of x-rays. These x-rays are measurable and result in structural data of the lattice [176]. Two methods exist to excite the electrons on an atom. One method makes use of an electron beam, as is used in scanning electron microscopes. The second method makes use of x-rays, known as energy-

Table 6: Summary of SEM and TEM observations for clay-based nanocomposites.

Method	Material	Synthesis method	Observations	References
SEM and TEM	Polypropylene-Polypropylene-grafted-maleic anhydride-montmorillonite clay nanocomposites (PP + PP-g-MA/MMT)	Melt mix extrusion	(i) Foaming cell size decreases as cell density increases with increase in MMT content.	[171]
	Physically crosslinked polyvinyl alcohol/bentonite nanocomposite hydrogel	Freeze-thawing technique	(ii) Pore walls thicken in the nanocomposite compared to lean PVA	[172]
	Polyaniline-clay hybrid nanocomposite (PANI/Clay)	In situ polymerization	(iii) Denser regions indicating intercalation of polymer	[173]
	Post-consumer propylene/Tunisian clay nanocomposite (PCPP/Clay)	Twin-screw extrusion	(iv) Clay finely distributed in the polymer matrix,	[174]

dispersive x-rays (EXD). Whichever the source, interactions within the atoms remain the same. If the emitted rays obey Bragg's law illustrated in equation (17), the waves reflect constructively thus amplifying their signal [177]. Energy-dispersive x-ray diffraction is very sensitive to the texture of the material to be analyzed. A poorly textured sample results in noisy data, making it difficult to identify crystal lattices. The main considerations for the sample are stability in vacuumized environments and sample contamination [177]. Kumar et al. [119] used EXD to authenticate the adsorption of Cr (III) ions on the surface of the cellulose-clay nanocomposite. XRD patterns from the same study indicated the crystalline structure of the composite.

$$n\lambda = 2d \sin\theta. \tag{18}$$

In a study by Rafiei et al. [178], a poly (acrylic acid)/bentonite nanocomposite was characterized using XRD, and the interpreted diffractograms translated that polyacrylic acid (PAA) and cetyltrimethylammonium (CTA) surfactants had evenly intercalated in the mineral layers of montmorillonite of the bentonite clay. The structure of the material was therefore an intercalated nanocomposite. XRD diffractograms for bentonite clay analyzed by [165] have shown a basal peak corresponding to montmorillonite in a study to synthesize a clay-hydrogel nanocomposite for Pb^{2+} ad Cd^{2+} removal. This basal peak was reported to disappear in the diffractogram of the nanocomposite due to exfoliation of the clay structure. Other reports on XRD analysis are summarized in Table 7.

7.3. Fourier Transform Infrared Spectroscopy (FTIR). The infrared region of the electromagnetic spectrum spans between 12800 cm^{-1} and 10 cm^{-1}. It is therefore divided into three categories, namely near-infrared region (12800 ~ 4000 cm^{-1}), middle infrared region (4000~200 cm^{-1}), and far-infrared region (50~1000 cm^{-1}). Since IR spectroscopy depends on vibrational movements of molecules with dipole moments, homonuclear diatomic molecules are not detectable with this method. The technique works on the mechanism that when infrared energy is irradiated through a sample, molecules absorb the energy at various wavelengths, and some transform to excited states. The wavelengths at which the absorption occurs are detected and peaks tabulated. Molecules can have multiple absorption peaks based on the vibrational freedom in the molecules [180]. Organic and inorganic peaks are mostly found within the 4000 ~ 400 cm^{-1} region [180]. To characterize polymer-clay nanocomposites, it is important to analyze lean clay first to detect clay peaks, corresponding to Si–O bonds. Peaks are expected to sharpen when an intercalant is added to the clay matrix [181]. Cole [181] used this method to study the degree of intercalation between propylene and montmorillonite clay particles.

In the study by Rafiei et al. [178], FTIR technique was also used in the characterization and it confirmed the XRD data that the CTA and PAA functional groups had intercalated into the clay interlayers. Unuabonah et al. [182] fabricated a PVA-modified kaolinite clay nanocomposite for the removal of Pb^{2+} and Cd^{2+} ions, and the FTIR analysis of the material shows the presence of –OH functional groups on its surface. Adsorption criteria were shown to be based on "inner-sphere surface complexation mechanism," according to FTIR data, and this increased metal ion adsorption almost three times [144]. In an FTIR characterization of polyacrylamide/bentonite hydrogel synthesized for the adsorption of Pb^{2+} and Cd^{2+}, it was reported that a C–N group peak observed prior to heavy metal adsorption shifted to a lower wave number with decreased sharpness when loaded with heavy metal ions. This illustrated an interaction between heavy metal ions and the C–N functional group in the nanocomposite [165]. Other reports in FTIR analysis are summarized in Table 8.

7.4. Thermogravimetric Analysis. Thermogravimetric analysis (TGA) is a method used to investigate the changes in mass of a material owing to thermodynamic reactions taking place in the material. The mass of the investigated material is continuously monitored as the temperature changes over time. Thereby, physical parameters, such as desorption, adsorption, absorption, and phase transitions, and chemical parameters, such as solid-gas reactions, thermal decomposition, and chemisorption, are investigated [185]. Three types of TGA exist as isothermal, quasistatic, or dynamic thermogravimetry. Isothermal, also known as static TGA, involves use of a constant temperature as change in mass is recorded inferring to time. Quasistatic TGA involves changing the temperature sequentially ensuring the sample stabilizes before the following rise. Dynamic TGA involves a linear change in temperature [186]. TGA is measured by the use of a thermogravimetric analyzer, consisting of a highly

Table 7: Summary of XRD observations in clay-based nanocomposites.

Method	Material	Synthesis method	Observations	References
XRD	Bimetallic-doped hybrid kaolinite nanocomposite	Solvothermal process	(i) Cu-doped compound showed an atacamite monoclinic polymorph (ii) Cu/Zn-doped composite showed a rhombohedral atacamite mineral.	[179]
	Nanocrystalline cellulose/bentonite nanocomposite (NCC-Bentonite)	Solution blending	(i) Confirmation of montmorillonite peaks in bentonite ($2\theta = 19.7^\circ$ and 22°) and cellulose in NCC ($2\theta = 22.3^\circ$).	[151]
	Polypropylene-Polypropylene-grafted-maleic anhydride-montmorillonite clay nanocomposites (PP + PP-g-MA/MMT)	Melt mix extrusion	(i) The characteristic peaks of MMT at $2\theta = 19.7^\circ$ and 22° decrease in intensity	[171]
	Physically crosslinked polyvinyl alcohol/ bentonite nanocomposite hydrogel	Freeze-thawing technique,	(i) Absence of a peak at $2\theta = 2$–10° indicates a possibility of exfoliation or mixed intercalated-exfoliated layers of clay in polymer matrix (ii) Characteristic peaks of semicrystalline PVA appear at 19.8° and 22.9°	[172]
	Post-consumer propylene/Tunisian clay nanocomposite	Twin-screw extrusion	(i) Characteristic peaks of kaolinite identified at 7.17, 1.49, and 2.56 Å (ii) Impurities identified at 3.03 Å (calcite) and 3.33 Å (quartz) (iii) Characteristic peak of Tunisian clay at 7.12 Å retained.	[174]
	Polyacrylonitrile vinyl triethoxysilane-sepiolite nanocomposite	Chemical grafting	(i) Peak of unmodified clay observed at $2\Theta = 8.215^\circ$ and 13.95° shifting to 8.87° and 13.45°, respectively, on modification. Modified sepiolite peaks at 40.01° and 49.91°.	[161]

Table 8: Summary of FTIR observations in clay-based nanocomposites.

Method	Material	Synthesis method	Observations	References
FTIR	Carboxymethyl chitosan/poly (ethylene glycol) bentonite nanocomposite (CMCh/PEG/MMT)	In situ polymerization	(i) Broad bands between 3600 and 3200 cm^{-1} due to –OH and –NH groups	[183]
	Nanocrystalline cellulose/bentonite nanocomposite (NCC-Bentonite)	Solution blending	(i) Cellulose characteristic peaks at 1045 (C–O/ C–C),1357 (C–H), and 2841 (CH2) (ii) Montmorillonite characteristic peaks at 3612 (Al(Mg)–OH), 3441 (H–O–H), 1641 (-OH bending), and 1041 cm^{-1} (Si–O–Si stretch) in bentonite	[151]
	Alginate/nano-cloisite nanocomposite hydrogel	Electron beam irradiation	(i) Strong peak observed at 1071 cm^{-1} related to the overlap of C–C bonds of alginate and Si–O–Si axial plane in clay.	[184]
	Polyaniline-clay hybrid nanocomposite (PANI/Clay)	In situ polymerization	(i) PANI/Clay peaks at 1241 cm^{-1} and 1304 cm^{-1} characteristic of PANI polymer.	[173]
	Post-consumer propylene/lay nanocomposite	Twin-screw extrusion	(i) Raw clay showed quartz (impurity) characteristic peak at 420 cm^{-1}. (ii) At 1433, 711.6, and 871.6 cm^{-1}, carbonate (dolomite (Ca, Mg $(CO_3)_2$) or calcite ($CaCO_3$)) are observed. (iii) Smectite phase with dioctaedric character is observed at 3627 and 912.1 cm^{-1}, attributed to Al–Al–OH- stretch.	[174]
	Polyacrylonitrile vinyl triethoxysilane-sepiolite nanocomposite	Chemical grafting	(i) Characteristic sepiolite peaks at 643, 691, and 976 cm^{-1} in lean characteristic nitrile group peak appeared at 2245 cm^{-1}.erpiolite clay. (ii) New peaks at 1391, 2810, and 2970 cm^{-1}(C–H vinyl group) (iii) Characteristic nitrile group peak appeared at 2245 cm^{-1}	[161]

Table 9: Summary of TGA observations in clay-based nanocomposites.

Method	Material	Synthesis method	Observations	References
TGA	Polypropylene-polypropylene-grafted-maleic anhydride-montmorillonite clay nanocomposites (PP + PP-g-MA/MMT)	Melt mix extrusion	(i) Thermal stability for nanocomposite was higher than lean polymer	[171]
	Physically crosslinked polyvinyl alcohol/bentonite nanocomposite hydrogel	Freeze-thawing technique	(i) Filler content (clay) increased melting and crystallization enthalpies in the PVA.	[172]
	Polyaniline/Clay nanocomposite	In situ polymerization	(i) Material with adsorbed heavy metal exhibited lower decomposition temperature than in desorbed state. Metal ion reduced the material's thermal stability.	[173]
	Post-consumer propylene/Tunisian clay nanocomposite (PCPP/Clay)	Twin-screw extrusion	(i) Increase in clay content increased the thermal stability of the nanocomposite.	[174]
	Polyacrylonitrile vinyl triethoxysilane-sepiolite nanocomposite	Chemical grafting	(i) Thermal stability of nanocomposite reinforced by clay	[161]

sensitive precision balance and a furnace with programmable temperature control. Thermal reactions are caused often by a constant rise in temperature. The atmosphere can either include vacuum, ambient air, inert gas, corrosive gas, reducing/oxidizing gases or carburizing gases. The pressures are varied too, ranging from controlled, constant, or high pressures [187]. TGA data are usually plotted into mass or initial mass versus time or temperature. Such data form a TGA curve. In some instances, a first derivative of the curve known as the DTG is plotted to show peaks of inflections, useful in differential thermal analysis [188]. TGA is used in analysis such as paints, thermoplastics, thermosets, composites, coatings, fuels, among others [186].

In a TGA analysis of geopolymer clay nanocomposite, Maleki et al. [189] reported an initial mass loss at 80–200°C owing to water evaporation and a second one in the region 400–700°C attributed to water loss due to clay's dihydroxylation. Kalantari and Afifi [190] reported an initial 15% mass loss at 40–145°C when studying the thermal stability of chitosan/polyvinyl alcohol/talc nanocomposite. The nanocomposite was reported to be more thermally stable compared to PVA and chitosan, enabling the material to decompose at 800°C. When polymers are reinforced with clay materials, they exhibit higher thermal stability. Malayoglu [191] reported an increase in thermal stability of chitosan when reinforced with montmorillonite clay in a nanocomposite. The author attributed the observation to surfactant interaction with chitosan-clay acting as a barrier in the chitosan decay process. Abdeldaym et al. [192] reported a similar phenomenon when using a polypyrrole/natural clay nanocomposite. Plain polypyrrole decomposed at about 204°C whose decomposition was pushed higher by the addition of clay to 226°C. El-Aziz et al. [193] also reported that cellulose grafted in the presence of clay showed higher thermostability in response to the presence of clay mineral structures. Other reports in TGA analysis are summarized in Table 9.

7.5. Brunauer–Emmett–Teller Analysis. Brunauer–Emmett–Teller (BET) is used in the measurement of pore size and surface area of solid materials in adsorption of gas molecules (nitrogen gas adsorption is often used as a standard). Data arising from BET analysis give insight into the physical structure of the material, in addition to moisture retention, shelf life, dissolution rate, and catalytic activity [194]. The analysis process involves bringing the sample's temperatures to near cryogenic using liquid nitrogen. Then nitrogen gas acting as an adsorbate is fed to the solid sample in controlled measures, with relative pressure equilibrating and weight W, of nitrogen adsorbed measured after each increment. An equation is known as the BET equation (Equation 19) allows a linear plot of $1/(P_0/P - 1)$ versus (P/P_0), which limits adsorption to a region in the (P/P_0) range of 0.05–0.35. By use of the plot, the weight, W_m, of nitrogen adsorbed is determined, which represents a monolayer surface coverage. The slope of the equation and its interception give the cumulative surface area of the sample [194].

$$\frac{1}{W\left(\left(P_0/P\right) - 1\right)} = \frac{1}{W_m C} + \left(\frac{C - 1}{W_m C}\right)\frac{P}{P_0}, \tag{19}$$

where C is the BET constant and is related to the adsorption energy corresponding to the first layer of adsorption. The value of C indicates the magnitude of adsorbate/adsorbent interactions. This method of analysis is most preferable for materials that exhibit Type II or Type IV adsorption isotherm behaviors. These materials showcase sufficient interactions between the adsorbate and the adsorbent and therefore give reliable data [195].

In a study by Maleki et al. [189] investigating the surface area and pore volume of a magnetic geopolymer/bentonite nanocomposite, the authors reported a greater surface area in the composite compared to the plain geopolymer and a slight decrease in the pore volume of the nanocomposite. This was attributed to the loading of the magnetizing Fe_3O_4 nanoparticles. Batool et al. [196] reported similar findings for pore volume when analyzing a polyacrylonitrile/cloisite nanocomposite. Malayoglu [191] reported a decrease in BET surface area of chitosan/montmorillonite nanocomposite attributing it to compacting in clay's interlayers, of the chitosan molecules thereby blocking nitrogen passage. This research agreed with Batool et al. [196] that the average diameter of the pores of the nanocomposites involved was higher compared to the respective non-composited

Table 10: Summary of BET observations in clay-based nanocomposites.

Method	Material	Synthesis method	Observations	References
BET	Polyaniline-clay hybrid nanocomposite (PANI/Clay)	In situ polymerization	(i) Surface area and total pore volume increased with PANI intercalation	[173]
	Polyacrylonitrile vinyl triethoxysilane-sepiolite nanocomposite	Chemical grafting	(i) Pore volume decreased on *vinyltriethoxysilane*modification, which further decreased on grafting with polyacrylonitrile	[161]
	Montmorillonite cellulose nanocomposite	Solution blending	(i) The BET surface area and pore volume of clay reduced on cellulose intercalation, as the pore diameter had a tremendous increment	[197]
	Acid-activated montmorillonite (AA-MMT)/polyethersulfone (PES) nanocomposite membrane	Phase inversion method	(i) Increase in AA-MMT in the matrix had an increase effect on the distribution of pore sizes and volumes.	[138]
	Smectite titanium ultrafiltration membrane nanocomposite (Sm/Z UF)	Layer-by-layer technique	(i) Increase in pore size distribution observed was attributed to densification of inner and outer parts of the membrane thus increasing its porosity.	[198]

compared materials. Other reports in FTIR analysis are summarized in Table 10.

8. Areas for Future Research

Based on the work reviewed herein, following areas have been identified for future research:

(i) Mechanism of intercalation of biopolymers and clay structures.

(ii) Modification of clay-based nanocomposites to remove both organic and inorganic contaminants interchangeably.

(iii) Application of heavy metal adsorbents in real contaminated water instead of simulated specifically contaminated wastewater.

(iv) Performance comparison of low-cost adsorbents and existing adsorption technologies.

(v) Studies on large-scale applicability of clay-based adsorbents in the decontamination of water.

(vi) Comparative study of regenerative capability and sludge production and ease of disposal between the existing adsorption technologies and clay-based nanocomposites.

(vii) In-depth study of the active life cycle and sustainability of clay-based nanocomposites especially in developing countries.

9. Conclusions

In light of this review, it was concluded that:

(i) Clay-based nanocomposites mostly exhibit heterogeneous adsorption, although some nanocomposites exhibit homogeneous adsorption.

(ii) In the fabrication of clay-based nanocomposites, high swelling clays, especially smectites, are of great significance because of their increased surface area.

(iii) These nanocomposites have yet low to none industrial utilization, in as much as they portray high efficiency in heavy metal removal.

(iv) Polymer intercalation into clay increases the surface area of the clay.

(v) Clay as a filler material increases the heat retardancy of polymers in which it is incorporated.

Data Availability

The data can be accessed in the cited papers in the review article.

Conflicts of Interest

The authors declare that there are no conflicts of interest regarding the publication of this article.

Acknowledgments

The authors of this work acknowledge every author of the works cited in this review.

References

[1] O. N. Borisova, I. G. Doronkina, and V. M. Feoktistova, "Resource-saving nanotechnologies in waste water treatment," *Nanotechnologies in Construction*, vol. 13, no. 2, pp. 124–130, 2021.

[2] F. Aquastat, "Global information system on water and agriculture: water resources," 2020, https://www.fao.org/aquastat/en/.

[3] UpKeep, "Most Interesting Statistics and Facts about Wastewater Management? Stats And Facts Watewater," 2019, https://www.upkeep.com/answers/maintenance-technicians/stats-and-facts-waste-water.

[4] World Health Organization, "1 in 3 people globally do not have access to safe drinking water," 2020, https://www.who.int/news/item/18-06-2019-1-in-3-people-globally-do-not-have-access-to-safe-drinking-water-unicef-who.

[5] G. White and M. Damon, "Finance for water is an investment in the future," 2016, https://water.org/our-impact/all-stories/finance-water-investment-future/.

[6] P. Environment Monitor, "Water Pollution- Sources of Water Pollution," 2017, http://www.environmentlaw.org.uk/rte.asp?id=90.

[7] J. A. Nathanson, "Wastewater Treatment," 2021, https://www.britannica.com/technology/wastewater-treatment.
[8] U. Epa, "Water: monitoring and assessment," *Monitoring And Assessing Water Quality—Volunteer Monitoring*, 2012, https://archive.epa.gov/water/archive/web/html/index-18.html.
[9] H. Hamdhani, D. E. Eppehimer, and M. T. Bogan, "Release of treated effluent into streams: a global review of ecological impacts with a consideration of its potential use for environmental flows," *Freshwater Biology*, vol. 65, no. 9, pp. 1657–1670, 2020.
[10] UNICEF, *Kenya's Water Crisis—Kenya's Water in 2020*, UNICEF, New York, NY, USA, 2020.
[11] J. D. Edwards, *Industrial Wastewater Treatment*, CRC Press, Boca Raton, FL, USA, 2019.
[12] M. A. Evans, "The sewage crisis in America," 2015, https://www.theatlantic.com/technology/archive/2015/09/americas-sewage-crisis-public-health/405541/.
[13] J. Peccia and P. Westerhoff, "We should expect more out of our sewage sludge," *Environmental Science and Technology*, vol. 49, no. 14, pp. 8271–8276, 2015.
[14] G. K. Kinuthia, V. Ngure, D. Beti, R. Lugalia, A. Wangila, and L. Kamau, "Levels of heavy metals in wastewater and soil samples from open drainage channels in Nairobi, Kenya: community health implication," *Scientific Reports*, vol. 10, no. 1, pp. 1–13, 2020.
[15] LennTech, "Heavy metals," 2017, https://www.lenntech.com/processes/heavy/heavy-metals/heavy-metals.htm.
[16] G. A. Engwa, P. U. Ferdinand, F. N. Nwalo, and M. N. Unachukwu, "Mechanism and Health Effects of Heavy Metal Toxicity in Humans," in *Poisoning In the Modern World—New Tricks For an Old Dog?*, O. Karcioglu and B. Arslan, Eds., 1st ed., pp. 77–95, IntechOpen, London, UK, 2019.
[17] M. Jaishankar, T. Tseten, N. Anbalagan, B. B. Mathew, and K. N. Beeregowda, "Toxicity, mechanism and health effects of some heavy metals," *Interdisciplinary Toxicology*, vol. 7, no. 2, p. 60, 2014.
[18] S. Sauvé, "Time to revisit arsenic regulations: comparing drinking water and rice," *BMC Public Health*, vol. 14, no. 1, pp. 1–5, 2014.
[19] S. J. S. Flora, "Arsenic-induced oxidative stress and its reversibility," *Free Radical Biology and Medicine*, vol. 51, no. 2, pp. 257–281, 2011.
[20] M. S. Mani, S. P. Kabekkodu, M. B. Joshi, and H. S. Dsouza, "Ecogenetics of lead toxicity and its influence on risk assessment," *Human & Experimental Toxicology*, vol. 38, no. 9, pp. 1031–1059, 2019.
[21] P. B. Tchounwou, C. G. Yedjou, A. K. Patlolla, and D. J. Sutton, "Heavy metal toxicity and the environment," *EXS*, vol. 101, pp. 133–164, 2012.
[22] P. Senthil Kumar and E. Gunasundari, "Bioremediation of heavy metals," in *Energy, Environment, and Sustainability*, A. K. Agarwal, Ed., 1st ed., pp. 165–195, Springer, Berlin, Germany, 2018.
[23] Z. Fu and S. Xi, "The effects of heavy metals on human metabolism," *Toxicology Mechanisms and Methods*, vol. 30, 2020.
[24] T. S. Anirudhan and S. Rijith, "Synthesis and characterization of carboxyl terminated poly(methacrylic acid) grafted chitosan/bentonite composite and its application for the recovery of uranium(VI) from aqueous media," *Journal of Environmental Radioactivity*, vol. 106, no. 7, pp. 8–19, 2012.
[25] Health and Environment, "Components of Waste Water Barnstable County," 2018, https://www.barnstablecountyhealth.org/health-topics/wastewater/components-of-waste-water.
[26] E. D. G. J. Owusu-Ansah, A. Sampson, S. K. Amponsah, R. C. Abaidoo, and T. Hald, "Performance, compliance and reliability of Waste stabilization pond: effluent discharge quality and environmental protection agency standards in Ghana," *Research Journal of Applied Sciences, Engineering and Technology*, vol. 10, no. 11, pp. 1293–1302, 2015.
[27] M. F. Montes, "Biochemical oxygen demand," in *Encyclopedia of Earth Sciences Series*, Springer, Berlin, Germany, 2016.
[28] A. Bezsenyi, G. Sági, M. Makó, L. Wojnárovits, and E. Takács, "The effect of hydrogen peroxide on the biochemical oxygen demand (BOD) values measured during ionizing radiation treatment of wastewater," *Radiation Physics and Chemistry*, vol. 189, Article ID 109773, 2021.
[29] I. Skoczko, J. Struk-Sokołowska, and P. Ofman, "Seasonal changes in nitrogen, phosphorus, BOD and COD removal in Bystre wastewater treatment plant," *Journal of Ecological Engineering*, vol. 18, pp. 185–191, 2017.
[30] H. Nezhadheydari, R. Tavabe, A. Mirvaghefi, A. Heydari, and M. Frinsko, "Effects of different concentrations of Fe 3 O 4 @ZnO and Fe 3 O 4 @CNT magnetic nanoparticles separately and in combination on aquaculture wastewater treatment," *Environmental Technology & Innovation*, vol. 15, Article ID 100414, 2019.
[31] S. Pavithra and S. Shanthakumar, "Removal of COD, BOD and color from municipal solid waste leachate using silica and iron nano particles-A comparative study," *Global NEST Printed in Greece. All Rights Reserved Pavithra S. and Shanthakumar S*, vol. 19, pp. 122–130, 2017.
[32] M. Gharloghi, A. Yazdanbakhsh, A. Eslami, and E. Aghayani, "Efficiency of iron oxide nanoparticles in advanced treatment of secondary effluent of municipal wastewater treatment plant," *Journal of Mazandaran University of Medical Sciences*, vol. 26, no. 135, pp. 130–143, 2016.
[33] S. Allen, G. Barren, O. Bath, C. Boone, L. Breckinridge, and M. Calloway, "Total Suspended Solids And Water Quality. Kentucky Water Watch," 2012, http://www.state.ky.us/nrepc/water/ramp/rmtss.htm.
[34] M. Haeffner, M. Schwientek, S. R. Jacobs et al., "Monitoring of suspended sediments in a tropical forested landscape with citizen science," *Frontiers in Water*, vol. 1, Article ID 656770, 2021.
[35] M. U. S. G. S. Nolan, "Turbidity and Water Water Science School," 2018, https://www.usgs.gov/special-topics/water-science-school/science/turbidity-and-water.
[36] S. Heger, "An installers guide to total suspended solids. onsite installer," 2017, https://www.onsiteinstaller.com/online_exclusives/2017/09/an_installers_guide_to_total_suspended_solids.
[37] I. Fondriest Environmental, "Turbidity, total suspended solids & water clarity. fundamentals of environmental measurements," 2014, https://www.fondriest.com/environmental-measurements/parameters/water-quality/turbidity-total-suspended-solids-water-clarity/#Turbid22.
[38] T. Amerian, R. Farnood, S. Sarathy, and D. Santoro, "effects of total suspended solids, particle size, and effluent temperature on the kinetics of peracetic acid decomposition in municipal wastewater," *Water Science and Technology*, vol. 80, 2019.
[39] T. Asano, R. G. Smith, and G. Tchobanoglous, "Municipal wastewater: treatment and reclaimed water characteristics,"

in *Irrigation with Reclaimed Municipal Wastewater–A Guidance Manual,* CRC Press, Boca Raton, FL, USA, 2019.
[40] D. Mara, "Domestic wastewater treatment in developing countries," in *Domestic Wastewater Treatment in Developing Countries*, D. Duncan, Ed., RoutledgeMilton Park, UK, 2013.
[41] K. Gaurab, "Physical, chemical and biological characteristics of sewage," 2019, https://www.onlinebiologynotes.com/physical-chemical-and-biological-characteristics-of-sewage/.
[42] T. Asano, R. G. Smith, and G. Tchobanoglous, "Municipal wastewater: treatment and reclaimed water characteristics," in *Irrigation with Reclaimed Municipal Wastewater–A Guidance Manual*, G. S. Pettygrove and T. Asano, Eds., CRC Press, Boca Raton, FL, USA, pp. 2-1–2–26, 2018.
[43] B. A. Hauser, "Chemical oxygen demand," in *Practical Manual of Wastewater Chemistry*, pp. 69–72, CRC Press, Boca Raton, FL, USA, 2018.
[44] D. P. Whitehead, "Total organic carbon (TOC) analysis and measurement | ELGA LabWater," 2021, https://www.elgalabwater.com/blog/total-organic-carbon-toc.
[45] Bloganica, "Primary, secondary, and tertiary wastewater treatment: how do they work? - innovative solutions for wastewater treatment | organica water inc.organica water," 2017, https://www.organicawater.com/primary-secondary-tertiary-wastewater-treatment-work/.
[46] S. Oakley, "Preliminary treatment and primary sedimentation," in *Water and Sanitation for the 21st Century: Health and Microbiological Aspects of Excreta and Wastewater Management (Global Water Pathogen Project)*, J. R. Mihelcic and M. E. Verbyla, Eds., Carlifornia State University, Long Beach, CA, USA, 2019.
[47] M. Eddy, M. Abu-Orf, G. Bowden et al., *Wastewater Engineering: Treatment and Resource Recovery*, McGraw Hill Education, New York, NY, USA, 2014.
[48] M. Farrokhi, M. Naimi-Joubani, A. Dargahi, M. Poursadeghiyan, and H. Ali Jamali, "Investigating activated sludge microbial population efficiency in heavy metals removal from compost leachate," *Polish Journal of Environmental Studies*, vol. 27, no. 2, pp. 623–627, 2018.
[49] C. P. Gerba and I. L. Pepper, "Municipal wastewater treatment," *Environmental and Pollution Science*, pp. 393–418, 2019.
[50] J. A. Nathanson, R. Curley, S. Sinha et al., "Wastewater treatment | process, history, importance, systems, & technologies. Encyclopedia Britannica," 2021, https://www.britannica.com/technology/wastewater-treatment.
[51] S. Kusuma, "Performance evaluation of wastewater treatment plant," *International Journal of Engineering Science and Technology*, vol. 2, no. 12, pp. 7785–7796, 2010.
[52] J. H. J. M. van der Graaf, J. de Koning, A. Ravazzini, and V. Miska, "Treatment matrix for reuse of upgraded wastewater," *Water Science and Technology: Water Supply*, vol. 5, no. 1, pp. 87–94, 2005.
[53] P. Ranjit, V. Jhansi, and K. V. Reddy, "Conventional wastewater treatment processes," in *Advances in the Domain of Environmental Biotechnolog*, N. R. Maddela, L. G. Cruzatty, and S. Chakraborty, Eds., 1st ed., pp. 455–479, Springer, Berlin, Germany, 2021.
[54] L. Rodriguez-Freire, J. Gonzalez-Estrella, and G. Li, "Technologies for fractionation of wastewater and resource recovery," in *Wastewater Treatment Residues as Resources for Biorefinery Products and Biofuels*, J. A. Olivares, D. Puyol, and J. Dufour, Eds., pp. 329–354, Elsevier, Amsterdam, Netherlands, 2019.
[55] M. M. Benjamin and D. F. Lawler, *Water Quality Engineering: Physical/Chemical Treatment Processes*, John Wiley & Sons, Hoboken, NJ, USA, 2013.
[56] Y. Dahman, K. Deonanan, T. Dontsos, and A. Lammatteo, *Nanopolymers Nanotechnology and Functional Materials for Engineer*, Elsevier, Amsterdam, Netherlands, 2017.
[57] L. P. Wang and Y. J. Chen, "Sequential precipitation of iron, copper, and zinc from wastewater for metal recovery," *Journal of Environmental Engineering*, vol. 145, no. 1, Article ID 04018130, 2019.
[58] H. Li, H. Zhang, J. Long, P. Zhang, and Y. Chen, "Combined Fenton process and sulfide precipitation for removal of heavy metals from industrial wastewater: bench and pilot scale studies focusing on in-depth thallium removal," *Frontiers of Environmental Science & Engineering*, vol. 13, no. 4, 2019.
[59] A. E. Lewis, "Review of metal sulphide precipitation," *Hydrometallurgy*, vol. 104, pp. 222–234, 2010.
[60] A. N. Zainuddin, T. Azwan Raja Mamat, H. Imam Maarof, S. Wahidah Puasa, and S. Rohana Mohd Yatim, "Removal of nickel, zinc and copper from plating process industrial raw effluent via hydroxide precipitation versus sulphide precipitation," *IOP Conference Series: Materials Science and Engineering*, vol. 551, no. 1, Article ID 012122, 2019.
[61] P. N. L. Lens, R. J. W. Meulepas, R. Sampaio, M. Vallero, and G. Esposito, "Bioprocess engineering of sulfate reduction for environmental technology," in *Microbial Sulfur Metabolism*, C. Dahl and C. G. Friedrich, Eds., 1st ed.pp. 285–295, Springer, Berlin, Germany, 2008.
[62] M. Sethurajan, E. D. van Hullebusch, and Y. v. Nancharaiah, "Biotechnology in the management and resource recovery from metal bearing solid wastes: recent advances," *Journal of Environmental Management*, vol. 211, pp. 138–153, 2018.
[63] A. H. Kaksonen and J. A. Puhakka, "Sulfate reduction based bioprocesses for the treatment of acid mine drainage and the recovery of metals," *Engineering in Life Science*, vol. 7, no. 6, pp. 541–564, 2007.
[64] E. Sahinkaya, D. Uçar, and A. H. Kaksonen, "Bio-precipitation of metals and metalloids," *Sustainable Heavy Metal Remediation*, Springer, Berlin, Germany, 2017.
[65] Y. v. Nancharaiah, S. V. Mohan, and P. N. L. Lens, "Biological and bioelectrochemical recovery of critical and scarce metals," *Trends in Biotechnology*, vol. 34, no. 2, pp. 137–155, 2016.
[66] M. L. Merroun and S. Selenska-Pobell, "Bacterial interactions with uranium: an environmental perspective," *Journal of Contaminant Hydrology*, vol. 102, pp. 285–295, 2008.
[67] S. Chabalala and E. M. N. Chirwa, "Removal of uranium (VI) under aerobic and anaerobic conditions using an indigenous mine consortium," *Minerals Engineering*, vol. 23, no. 6, pp. 526–531, 2010.
[68] C. Zhou, A. Ontiveros-Valencia, L. Cornette de Saint Cyr et al., "Uranium removal and microbial community in a H2-based membrane biofilm reactor," *Water Research*, vol. 64, pp. 255–264, 2014.
[69] F. Fu and Q. Wang, "Removal of heavy metal ions from wastewaters: a review," *Journal of Environmental Management*, vol. 92, no. 3, pp. 407–418, 2011.
[70] B. Alyüz and S. Veli, "Kinetics and equilibrium studies for the removal of nickel and zinc from aqueous solutions by ion exchange resins," *Journal of Hazardous Materials*, vol. 167, pp. 482–488, 2009.
[71] S. A. Abo-Farha, A. Y. Abdel-Aal, I. A. Ashour, and S. E. Garamon, "Removal of some heavy metal cations by

synthetic resin purolite C100," *Journal of Hazardous Materials*, vol. 169, pp. 190–194, 2009.

[72] K. K. Kennedy, K. J. Maseka, M. Mbulo, K. K. Kennedy, K. J. Maseka, and M. Mbulo, "Selected adsorbents for removal of contaminants from wastewater: towards engineering clay minerals," *Open Journal of Applied Sciences*, vol. 8, no. 8, pp. 355–369, 2018.

[73] A. Mohammad-Khan and R. Ansari, "Activated charcoal: preparation, characterization and applications: a review article," *InternationAL Journal of ChemTech Research*, vol. 1, pp. 859–869, 2009.

[74] A. Bhatnagar and A. Minocha, "Conventional and non-conventional adsorbents for removal of pollutants from water," *Indian Journal of Chemical Technology*, vol. 13, pp. 203–217, 2006.

[75] T. Maruyama, "Carbon nanotubes," in *Handbook of Carbon-Based Nanomaterials*, S. Thomas, C. Sarathchandran, S. A. Ilangovan, and J. C. Moreno-Pirajan, Eds., 1st ed., pp. 299–319, Elsevier, Amsterdam, Netherlands, 2021.

[76] A. M. Holban, A. M. Grumezescu, and E. Andronescu, "Inorganic nanoarchitectonics designed for drug delivery and anti-infective surfaces," *Surface Chemistry of Nanobiomaterials: Applications of Nanobiomaterials*, pp. 301–327, 2016.

[77] H. Alijani and Z. Shariatinia, "Synthesis of high growth rate SWCNTs and their magnetite cobalt sulfide nanohybrid as super-adsorbent for mercury removal," *Chemical Engineering Research and Design*, vol. 129, pp. 132–149, 2018.

[78] H. A. Qdais and H. Moussa, "Removal of heavy metals from wastewater by membrane processes: a comparative study," *Desalination*, vol. 164, no. 2, pp. 105–110, 2004.

[79] B. S. Thaçi and S. T. Gashi, "Reverse osmosis removal of heavy metals from wastewater effluents using biowaste materials pretreatment," *Polish Journal of Environmental Studies*, vol. 28, no. 1, pp. 337–341, 2018.

[80] B. A. M. Al-Rashdi, D. J. Johnson, and N. Hilal, "Removal of heavy metal ions by nanofiltration," *Desalination*, vol. 315, pp. 2–17, 2013.

[81] G. Al-Enezi, M. F. Hamoda, and N. Fawzi, "Ion exchange extraction of heavy metals from wastewater sludges," *Journal of Environmental Science and Health - Part A: Toxic/Hazardous Substances and Environmental Engineering*, vol. 39, no. 2, pp. 455–464, 2004.

[82] J. M. Arana Juve, F. M. S. Christensen, Y. Wang, and Z. Wei, "Electrodialysis for metal removal and recovery: a review," *Chemical Engineering Journal*, vol. 435, Article ID 134857, 2022.

[83] N. A. A. Qasem, R. H. Mohammed, and D. U. Lawal, "Removal of heavy metal ions from wastewater: a comprehensive and critical review," *Npj Clean Water*, vol. 4, no. 1, pp. 1–15, 2021.

[84] R. C. Gumerman, R. L. Culp, and S. P. Hansen, "Estimating water treatment costs," 1979, http://nepis.epa.gov/Exe/ZyPDF.cgi/300009IH.PDF?Dockey=300009IH.PDF.

[85] P. Pandit, K. Singha, S. Maity, S. Maiti, and P. Kane, "Treatment of textile wastewater by agricultural waste biomasses," in *Sustainable Technologies for Textile Wastewater Treatments*, S. S. Muthu, Ed., 1st ed., pp. 137–156, Elsevier, Amsterdam, Netherlands, 2021.

[86] G. Crini, E. Lichtfouse, L. D. Wilson, and N. Morin-Crini, "Conventional and non-conventional adsorbents for wastewater treatment," *Environmental Chemistry Letters*, vol. 17, pp. 195–213, 2019.

[87] D. Park, Y. S. Yun, and J. M. Park, "The past, present, and future trends of biosorption," *Biotechnology and Bioprocess Engineering*, vol. 15, no. 1, pp. 86–102, 2010.

[88] I. Ali, "Water treatment by adsorption columns: evaluation at ground level," *Separation and Purification Reviews*, vol. 43, no. 3, pp. 175–205, 2014.

[89] A. Onur, A. Ng, W. Batchelor, and G. Garnier, "Multi-layer filters: adsorption and filtration mechanisms for improved separation," *Frontiers of Chemistry*, vol. 6, 2018.

[90] Y. Yigzaw, R. Piper, M. Tran, and A. A. Shukla, "Exploitation of the adsorptive properties of depth filters for host cell protein removal during monoclonal antibody purification," *Biotechnology Progress*, vol. 22, no. 1, pp. 288–296, 2006.

[91] A. A. Shukla and J. R. Kandula, "Harvest and recovery of monoclonal antibodies: cell removal and clarification," *Process Scale Purification of Antibodies*, vol. 21, pp. 53–78, 2008.

[92] A. Razzaz, S. Ghorban, L. Hosayni, M. Irani, and M. Aliabadi, "Chitosan nanofibers functionalized by TiO_2 nanoparticles for the removal of heavy metal ions," *Journal of the Taiwan Institute of Chemical Engineers*, vol. 58, no. 58, pp. 333–343, 2016.

[93] U. Fegade and G. Jethave, "Advances and applications," *Interface Science and Technology*, vol. 33, pp. 557–586, 2021.

[94] M. Asif, E. H. Al-Ghurabi, A. Ajbar, and N. S. Kumar, "Hydrodynamics of pulsed fluidized bed of ultrafine powder: fully collapsing fluidized bed," *Processes*, vol. 2020, 2020.

[95] G. Crini and P.-M. Badot, "Conventional and non-conventional sorbents for pollutant removal from wastewaters," in *Sorption Processes and Pollution*, Presses universitaires de Franche-Comté, Besançon, France, 2010.

[96] L. Pontoni and M. Fabbricino, "Use of chitosan and chitosan-derivatives to remove arsenic from aqueous solutionsâ€"a mini review," *Carbohydrate Research*, vol. 356, pp. 86–92, 2012.

[97] H. Hosseinzadeh and S. Ramin, "Effective removal of copper from aqueous solutions by modified magnetic chitosan/graphene oxide nanocomposites," *International Journal of Biological Macromolecules*, vol. 113, pp. 859–868, 2018.

[98] V. Gupta, P. Carrott, R. Singh, M. Chaudhary, and S. Kushwaha, "Cellulose: a review as natural, modified and activated carbon adsorbent," *Bioresource Technology*, vol. 216, 2016.

[99] S. Dridi-Dhaouadi, N. ben Douissa-Lazreg, and M. F. M'Henni, "Removal of lead and yellow 44 acid dye in single and binary component systems by raw posidonia oceanica and the cellulose extracted from the raw biomass," *Environmental Technology*, vol. 32, 2011.

[100] Z. Wu, Z. Cheng, and W. Ma, "Adsorption of Pb(II) from glucose solution on thiol-functionalized cellulosic biomass," *Bioresource Technology*, vol. 104, pp. 807–809, 2012.

[101] N. Anton, A. Uliana, M. Olga, A. Eugenia, and I. Y. Vladimir, "Physico chemical properties of montmorillonite clays and their application in clinical practice (review)," *Research Result: Pharmacology and Clinicl Pharmacology*, vol. 3, no. 2, pp. 119–128, 2017.

[102] H. Daumier, A. Savage, B. O. Sicyon, and A. Augustyn, Encyclopedia Britannica, "Clay," 2020, https://www.britannica.com/science/clay-geology.

[103] S. Barakan and V. Aghazadeh, "The advantages of clay mineral modification methods for enhancing adsorption efficiency in wastewater treatment: a review," *Environmental Science and Pollution Research*, vol. 28, 2021.

[104] M. Ghadiri, W. Chrzanowski, and R. Rohanizadeh, "Biomedical applications of cationic clay minerals," *RSC Advances*, vol. 5, no. 37, pp. 29467–29481, 2015.

[105] B. Karpiński and M. Szkodo, "Clay minerals—mineralogy and phenomenon of clay swelling in oil & gas industry," *Advances in Materials Science*, vol. 15, no. 1, pp. 37–55, 2015.

[106] Y. Khaledian, E. C. Brevik, P. Pereira, A. Cerdà, M. A. Fattah, and H. Tazikeh, "Modeling soil cation exchange capacity in multiple countries," *Catena*, vol. 158, pp. 194–200, 2017.

[107] K. G. Bhattacharyya and S. Gupta, "Adsorptive accumulation of Cd(II), Co(II), Cu(II), Pb(II) and Ni(II) ions from water onto Kaolinite: influence of acid activation," *Adsorption Science and Technology*, vol. 27, no. 1, pp. 47–68, 2009.

[108] L. de Pablo, M. L. Chávez, and M. Abatal, "Adsorption of heavy metals in acid to alkaline environments by montmorillonite and Ca-montmorillonite," *Chemical Engineering Journal*, vol. 171, no. 3, pp. 1276–1286, 2011.

[109] A. Sdiri, T. Higashi, T. Hatta, F. Jamoussi, and N. Tase, "Evaluating the adsorptive capacity of montmorillonitic and calcareous clays on the removal of several heavy metals in aqueous systems," *Chemical Engineering Journal*, vol. 172, no. 1, pp. 37–46, 2011.

[110] S. A. Al-Jlil, "Kinetic of adsorption of chromium and lead ions on bentonite clay using novel internal parallel model," *Research Journal of Environmental Toxicology*, vol. 9, no. 1, pp. 1–16, 2015.

[111] T. Zhang, W. Wang, Y. Zhao, H. Bai, T. Wen, and S. Kang, "Removal of heavy metals and dyes by clay-based adsorbents: from natural clays to 1D and 2D nano-composites," *Chemical Engineering Journal*, vol. 420, Article ID 127574, 2021.

[112] A. Awasthi, P. Jadhao, and K. Kumari, "Clay nano-adsorbent: structures, applications and mechanism for water treatment," *SN Applied Sciences*, vol. 1, no. 9, 2019.

[113] N. AlMasoud, M. Habila, Z. Alothman et al., "Nano-clay as a solid phase microextractor of copper, cadmium and lead for ultra-trace quantification by ICP-MS," *Analytical Methods*, vol. 12, no. 41, pp. 4949–4955, 2020.

[114] A. El Kassimi, Y. Achour, M. El Himri, R. Laamari, and M. El Haddad, "Removal of two cationic dyes from aqueous solutions by adsorption onto local clay: experimental and theoretical study using DFT method," *International Journal of Environmental Analytical Chemistry*, vol. 101, pp. 1–22, 2021.

[115] R. El Haouti, H. Ouachtak, A. El Guerdaoui et al., "Cationic dyes adsorption by Na-Montmorillonite Nano Clay: experimental study combined with a theoretical investigation using DFT-based descriptors and molecular dynamics simulations," *Journal of Molecular Liquids*, vol. 290, Article ID 111139, 2019.

[116] H. Masoudi, F. Ravari, and H. Mosaddeghi, "Removal of nitrate from water by modified nano-clay and comparison with nano-graphene, nano-Fe_3O_4 and nano-clay—isotherm and kinetics study," *Desalination and Water Treatment*, vol. 167, pp. 218–230, 2019.

[117] L. Rafati, M. Ehrampoush, A. Rafati, M. Mokhtari, and A. Mahvi, "Modeling of adsorption kinetic and equilibrium isotherms of naproxen onto functionalized nano-clay composite adsorbent," *Journal of Molecular Liquids*, vol. 224, pp. 832–841, 2016.

[118] K. Shapira and I. Zucker, "Emerging investigator series: molybdenum disulfide-enabled activated carbon—a multifunctional adsorbent for practical water treatment applications," *Environmental Sciences: Nano*, vol. 9, no. 2, pp. 477–488, 2022.

[119] A. S. K. Kumar, S. Kalidhasan, V. Rajesh, and N. Rajesh, "Application of cellulose-clay composite biosorbent toward the effective adsorption and removal of chromium from industrial wastewater," *Industrial & Engineering Chemistry Research*, vol. 51, no. 1, pp. 58–69, 2012.

[120] Q. Chen, R. Zhu, W. Deng et al., "From used montmorillonite to carbon monolayer–montmorillonite nanocomposites," *Applied Clay Science*, vol. 100, pp. 112–117, 2014.

[121] Y. Ma, L. Lv, Y. Guo et al., "Porous lignin based poly (acrylic acid)/organo-montmorillonite nanocomposites: swelling behaviors and rapid removal of Pb (II) ions," *Polymer*, vol. 128, pp. 12–23, 2017.

[122] A. Heydari, H. Khoshnood, H. Sheibani, and F. Doostan, "Polymerization of β-cyclodextrin in the presence of bentonite clay to produce polymer nanocomposites for removal of heavy metals from drinking water," *Polymers for Advanced Technologies*, vol. 28, no. 4, pp. 524–532, 2017.

[123] M. Irani, H. Ismail, Z. Ahmad, and M. Fan, "Synthesis of linear low-density polyethylene-g-poly (acrylic acid)-co-starch/organo-montmorillonite hydrogel composite as an adsorbent for removal of Pb (II) from aqueous solutions," *Journal of Environmental Sciences*, vol. 27, pp. 9–20, 2015.

[124] K. el Adraa, T. Georgelin, J.-F. Lambert, F. Jaber, F. Tielens, and M. Jaber, *Cysteine-montmorillonite composites for heavy metal cation complexation: a combined experimental and theoretical study*, Elsevier, 2017, https://www.google.com/search?rlz=1C1GCEB_enIN992IN992&q=Amsterdam&stick=H4sIAAAAAAAAAOPgE-LUz9U3MDJLSYpXYgcxs40LtLSyk63084vSE_MyqxJLMvPzUDhWGamJKYWliUUlqUXFi1g5HXOLgayUxNwdrIy72Jk4GAD1-FzrVgAAAA&sa=X&ved=2ahUKEwjxpbifpIr4AhXGwTgGHTjaBTAQmxMoAXoECGoQAw.

[125] C. M. Futalan, C. C. Kan, M. L. Dalida, K. J. Hsien, C. Pascua, and M. W. Wan, "Comparative and competitive adsorption of copper, lead, and nickel using chitosan immobilized on bentonite," *Carbohydrate Polymers*, vol. 83, no. 2, pp. 528–536, 2011.

[126] V. N. Tirtom, A. Dinçer, S. Becerik, T. Aydemir, and A. Çelik, "Comparative adsorption of Ni(II) and Cd(II) ions on epichlorohydrin crosslinked chitosan–clay composite beads in aqueous solution," *Chemical Engineering Journal*, vol. 197, pp. 379–386, 2012.

[127] M. Cittan, V. N. Tirtom, A. Dinçer, and A. Çelik, "Epichlorohydrin crosslinked chitosan–clay composite beads for on-line preconcentration and determination of chromium (III) by flow injection flame atomic absorption spectrometry," *Analytical Methods*, vol. 6, no. 14, pp. 5298–5303, 2014.

[128] T. S. Anirudhan and P. S. Suchithra, "Heavy metals uptake from aqueous solutions and industrial wastewaters by humic acid-immobilized polymer/bentonite composite: kinetics and equilibrium modeling," *Chemical Engineering Journal*, vol. 156, no. 1, pp. 146–156, 2010.

[129] K. El Adraa, T. Georgelin, J. F. Lambert, F. Jaber, F. Tielens, and M. Jaber, "Cysteine-montmorillonite composites for heavy metal cation complexation: a combined experimental and theoretical study," *Chemical Engineering Journal*, vol. 314, pp. 406–417, 2017.

[130] K. Kalantari, M. B. Ahmad, H. R. FardMasoumi, K. Shameli, M. Basri, and R. Khandanlou, "Rapid and high capacity adsorption of heavy metals by Fe3O4/montmorillonite nanocomposite using response surface methodology:

preparation, characterization, optimization, equilibrium isotherms, and adsorption kinetics study," *Journal of the Taiwan Institute of Chemical Engineers*, vol. 49, pp. 192–198, 2015.

[131] G. Zhao, H. Zhang, Q. Fan et al., "Sorption of copper(II) onto super-adsorbent of bentonite–polyacrylamide composites," *Journal of Hazardous Materials*, vol. 173, pp. 661–668, 2010.

[132] Á. García-Padilla, K. A. Moreno-Sader, Á. Realpe, M. Acevedo-Morantes, and J. B. P. Soares, "Evaluation of adsorption capacities of nanocomposites prepared from bean starch and montmorillonite," *Sustainable Chemistry and Pharmacy*, vol. 17, Article ID 100292, 2020.

[133] S. Yadav, V. Srivastava, S. Banerjee, F. Gode, and Y. C. Sharma, "Studies on the removal of nickel from aqueous solutions using modified riverbed sand," *Environmental Science and Pollution Research*, vol. 20, no. 1, pp. 558–567, 2013.

[134] X. Zhang and X. Wang, "Adsorption and desorption of nickel(II) ions from aqueous solution by a lignocellulose/montmorillonite nanocomposite," *PLoS One*, vol. 10, no. 2, Article ID e0117077, 2015.

[135] J. H. Hassen, "Montmorillonite nanoclay interaction with 2-aminophenol and 2-nitrophenol," *Research Journal of Pharmacy and Technology*, vol. 12, no. 6, pp. 2828–2831, 2019.

[136] R. Msaadi, G. Yilmaz, A. Allushi et al., "Highly selective copper ion imprinted clay/polymer nanocomposites prepared by visible light initiated radical photopolymerization," *Polymers*, vol. 11, 2019.

[137] K. Moreno-Sader, A. García-Padilla, A. Realpe, M. Acevedo-Morantes, and J. B. P. Soares, "Removal of heavy metal water pollutants ($Co2^{+}$ and $Ni2^{+}$) using polyacrylamide/sodium montmorillonite (PAM/Na-MMT) nanocomposites," *ACS Omega*, vol. 4, no. 6, pp. 10834–10844, 2019.

[138] M. Mahmoudian, P. G. Balkanloo, and E. Nozad, "A facile method for dye and heavy metal elimination by pH sensitive acid activated montmorillonite/polyethersulfone nanocomposite membrane," *Chinese Journal of Polymer Science*, vol. 36, no. 1, pp. 49–57, 2017.

[139] S. Wadhawan, A. Jain, J. Nayyar, and S. K. Mehta, "Role of nanomaterials as adsorbents in heavy metal ion removal from waste water: a review," *Journal of Water Process Engineering*, vol. 33, 2020.

[140] M. E. M. Hassouna, M. Shaban, and F. M. Nassif, "Removal of iron and manganese ions from ground water using kaolin sub micro powder and its modified forms," *International Journal of Bioassays*, vol. 3, no. 07, pp. 3137–3145, 2014, https://www.ijbio.com/articles/removal-of-iron-and-manganese-ions-from-groundwater-using-kaolin-sub-micropowder-and-its-modified-forms.pdf.

[141] A. E. A. Sallam, M. S. Al-Zahrani, M. I. Al-Wabel, A. S. Al-Farraj, and A. R. A. Usman, "Removal of Cr(VI) and toxic ions from aqueous solutions and tannery wastewater using polymer-clay composites," *Sustainability*, vol. 9, no. 11, 2017.

[142] R. Dubey, J. Bajpai, and A. K. Bajpai, "Chitosan-alginate nanoparticles (CANPs) as potential nanosorbent for removal of Hg (II) ions," *Environmental Nanotechnology, Monitoring & Management*, vol. 6, no. 6, pp. 32–44, 2016.

[143] E. J. Kim, C. S. Lee, Y. Y. Chang, and Y. S. Chang, "Hierarchically structured manganese oxide-coated magnetic nanocomposites for the efficient removal of heavy metal ions from aqueous systems," *ACS Applied Materials & Interfaces*, vol. 5, pp. 9628–9634, 2013.

[144] K. Ravikumar and J. Udayakumar, "Preparation and characterisation of green clay-polymer nanocomposite for heavy metals removal," *Chemistry and Ecology*, vol. 36, no. 3, pp. 270–291, 2020.

[145] Y. Xu, J. Chen, R. Chen, P. Yu, S. Guo, and X. Wang, "Adsorption and reduction of chromium(VI) from aqueous solution using polypyrrole/calcium rectorite composite adsorbent," *Water Research*, vol. 160, pp. 148–157, 2019.

[146] M. qin Jiang, X. ying Jin, X. Q. Lu, and Z. liang. Chen, "Adsorption of Pb(II), Cd(II), Ni(II) and Cu(II) onto natural kaolinite clay," *Desalination*, vol. 252, pp. 33–39, 2010.

[147] M. L. Masheane, L. N. Nthunya, S. S. Sambaza et al., "Chitosan-based nanocomposite beads for drinking water production," *IOP Conference Series: Materials Science and Engineering*, vol. 195, no. 1, Article ID 012004, 2017.

[148] N. N. Nassar, "Rapid removal and recovery of Pb(II) from wastewater by magnetic nanoadsorbents," *Journal of Hazardous Materials*, vol. 184, pp. 538–546, 2010.

[149] G. Murithi, C. O. Onindo, E. W. Wambu, and G. K. Muthakia, "Removal of cadmium (II) ions from water by adsorption using water hyacinth (*Eichhornia crassipes*) biomass," *Bioresources*, vol. 9, no. 2, pp. 3613–3631, 2014.

[150] A. O. Dada, A. P. Olalekan, and A. M. Olatunya, "Langmuir, Freundlich, Temkin and Dubinin–radushkevich Isotherms: studies of equilibrium sorption of Zn^{2+} unto phosphoric acid modified rice husk," *Journal of Applied Chemistry*, vol. 1, no. 3, pp. 38–45, 2012.

[151] J. N. Putro, S. P. Santoso, S. Ismadji, and Y. H. Ju, "Investigation of heavy metal adsorption in binary system by nanocrystalline cellulose—bentonite nanocomposite: improvement on extended Langmuir isotherm model," *Microporous and Mesoporous Materials*, vol. 246, pp. 166–177, 2017.

[152] M. Kragović, M. Stojmenović, J. Petrović et al., "Influence of alginate encapsulation on point of zero charge (pHpzc) and thermodynamic properties of the natural and Fe(III)—modified zeolite," *Procedia Manufacturing*, vol. 32, pp. 286–293, 2019.

[153] S. N. Ndung'u, T. Nyahanga, R. N. Wanjau, and E. W. Nthiga, "Adsorption evaluation of selected heavy metal ions by amino- functionalized low-cost adsorbents," *A Review*, vol. 9, no. 7, pp. 339–357, 2021.

[154] Y. Liu, G. Wang, Q. Luo, X. Li, and Z. Wang, "The thermodynamics and kinetics for the removal of copper and nickel ions by the zeolite Y synthesized from fly ash," *Materials Research Express*, vol. 6, no. 2, Article ID 025001, 2018.

[155] A. A. Inyinbor, F. A. Adekola, and G. A. Olatunji, "Kinetics, isotherms and thermodynamic modeling of liquid phase adsorption of Rhodamine B dye onto *Raphia hookeri* fruit epicarp," *Water Resources and Industry*, vol. 15, pp. 14–27, 2016.

[156] M. Sharma, J. Singh, S. Hazra, and S. Basu, "Adsorption of heavy metal ions by mesoporous ZnO and TiO2@ZnO monoliths: adsorption and kinetic studies," *Microchemical Journal*, vol. 145, pp. 105–112, 2019.

[157] E. P. de Sousa, D. T. de Araujo, V. G. Peixoto, B. F. Ferreira, E. H. de Faria, and E. F. Molina, "Effect of sodium bentonite content on structural-properties of ureasilpoly (ethylene oxide)-PEO hybrid: a perspective for water treatment," *Applied Clay Science*, vol. 191, Article ID 105605, 2020.

[158] P. Liu, L. Jiang, L. Zhu, and A. Wang, "Novel approach for attapulgite/poly(acrylic acid) (ATP/PAA) nanocomposite microgels as selective adsorbent for Pb (II) Ion," *Reactive and Functional Polymers*, vol. 74, no. 1, pp. 72–80, 2014.

[159] R. Ahmad and I. Hasan, "L-cystein modified bentonite-cellulose nanocomposite (cellu/cys-bent) for adsorption of Cu^{2+}, Pb^{2+}, and Cd^{2+} ions from aqueous solution," *Separation Science and Technology*, vol. 51, 2016.

[160] V. B. Yadav, R. Gadi, and S. Kalra, "Clay based nanocomposites for removal of heavy metals from water: a review," *Journal of Environmental Management*, vol. 232, pp. 803–817, 2019.

[161] F. Altaf, R. Batool, M. A. Ahmad, R. Raza, M. A. Khan, and G. Abbas, "Novel vinyl-modified sepiolite-based polymer nanocomposites: synthesis and characterization," *Iranian Polymer Journal (English Edition)*, vol. 27, no. 6, pp. 413–422, 2018.

[162] R. S. Hebbar, A. M. Isloor, B. Prabhu, A. M. Inamuddin Asiri, and A. F. Ismail, "Removal of metal ions and humic acids through polyetherimide membrane with grafted bentonite clay," *Scientific Reports*, vol. 8, no. 1, pp. 1–16, 2018.

[163] R. Chakraborty, A. Asthana, A. K. Singh, B. Jain, and A. B. H. Susan, "Adsorption of heavy metal ions by various low-cost adsorbents: a review," *International Journal of Environmental Analytical Chemistry*, vol. 102, pp. 342–379, 2020.

[164] G. Yeganeh, B. Ramavandi, H. Esmaeili, and S. Tamjidi, "Dataset of the aqueous solution and petrochemical wastewater treatment containing ammonia using low cost and efficient bio-adsorbents," *Data in Brief*, vol. 26, Article ID 104308, 2019.

[165] S. A. Khan, M. F. Siddiqui, and T. A. Khan, "Ultrasonic-assisted synthesis of polyacrylamide/bentonite hydrogel nanocomposite for the sequestration of lead and cadmium from aqueous phase: equilibrium, kinetics and thermodynamic studies," *Ultrasonics Sonochemistry*, vol. 60, Article ID 104761, 2020.

[166] D. Abunah, C. Onindo, D. Andala, and E. Ochoti, "Physico-chemical removal of heavy metals from contaminated water using recyclable montmorillonite cellulose nanocomposite," *Journal of Materials and Environmental Sciences*, vol. 10, no. 12, pp. 1349–1361, 2019, https://www.jmaterenvironsci.com/Document/vol10/vol10_N12/JMES-2019-10-133-Abunah.pdf.

[167] R. Mirsafaei and M. Kolahdoozan, "Preparation and characterization of poly (amide-ester-imide)/Na^{+}-MMT nanocomposite via ultrasonic method," *Journal of Polymer Engineering*, vol. 37, no. 5, pp. 443–448, 2017.

[168] Z. Cherifi, B. Boukoussa, A. Zaoui, M. Belbachir, and R. Meghabar, "Structural, morphological and thermal properties of nanocomposites poly(GMA)/clay prepared by ultrasound and in-situ polymerization," *Ultrasonics Sonochemistry*, vol. 48, pp. 188–198, 2018.

[169] Thermofisher, "Electron Microscopy | TEM vs SEM | thermo Fisher scientific - ecwhermo Fisher Scientific," 2019, http://www.thermofisher.com/ng/en/home/materials-science/learning-center/applications/sem-tem-difference.html.

[170] M. A. Khan, A. A. Alqadami, S. M. Wabaidur et al., "Oil industry waste based non-magnetic and magnetic hydrochar to sequester potentially toxic post-transition metal ions from water," *Journal of Hazardous Materials*, vol. 400, pp. 1–12, Article ID 123247, 2020.

[171] T. N. Moja, N. Bunekar, S. Mojaki et al., "Polypropylene-Polypropylene-Grafted-maleic anhydride-montmorillonite clay nanocomposites for Pb (II) removal," *Journal of Inorganic and Organometallic Polymers and Materials*, vol. 1, 2018.

[172] L. M. Sanchez, P. S. Shuttleworth, C. Waiman, G. Zanini, V. A. Alvarez, and R. P. Ollier, "Physically-crosslinked polyvinyl alcohol composite hydrogels containing clays, carbonaceous materials and magnetic nanoparticles as fillers," *Journal of Environmental Chemical Engineering*, vol. 8, no. 3, Article ID 103795, 2020.

[173] H. Soltani, A. Belmokhtar, F. Z. Zeggai, A. Benyoucef, S. Bousalem, and K. Bachari, "Copper(II) removal from aqueous solutions by PANI-clay hybrid material: fabrication, characterization, adsorption and kinetics study," *Journal of Inorganic and Organometallic Polymers and Materials*, vol. 29, no. 3, pp. 841–850, 2019.

[174] K. Zdiri, A. Elamri, M. Hamdaoui, N. Khenoussi, O. Harzallah, and J. Brendle, "Impact of Tunisian clay nanofillers on structure and properties of post-consumer polypropylene-based nanocomposites," *Journal of Thermoplastic Composite Materials*, vol. 32, no. 9, pp. 1159–1175, 2018.

[175] Y. Chen, Z. Guo, X. Wang, and C. Qiu, "Sample preparation," *Journal of Chromatography A*, vol. 1184, pp. 191–219, 2008.

[176] G. Piburn and A. R. Barron, "An introduction to energy dispersive X-ray spectroscopy," in *Physical Methods in Chemistry and Nano Science*, P. M. Raja and A. R. Barron, Eds., 2nd ed., pp. 3–139, Openstax, Houston, Tx, USA, 2012.

[177] B. Cantor, "Bragg's law," in *The Equations of Materials*, D. Henry, N. Eby, J. Goofge, and D. Mogk, Eds., 1st ed., pp. 24–44, Oxford University Press, Oxford, UK, 2020.

[178] H. R. Rafiei, M. Shirvani, and O. A. Ogunseitan, "Removal of lead from aqueous solutions by a poly (acrylic acid)/bentonite nanocomposite," *Applied Water Science*, vol. 6, no. 4, pp. 331–338, 2016.

[179] C. G. Ugwuja, O. O. Adelowo, A. Ogunlaja et al., "Visible-light-mediated photodynamic water disinfection @ bimetallic-doped hybrid clay nanocomposites [Research-article]," *ACS Applied Materials and Interfaces*, vol. 11, no. 28, pp. 25483–25494, 2019.

[180] N. Birkner, *How an Ftir Spectrometer Operates*, UC Davis ChemWiki, 2011.

[181] K. C. Cole, "Use of infrared spectroscopy to characterize clay intercalation and exfoliation in polymer nanocomposites," *Macromolecules*, vol. 41, no. 3, pp. 834–843, 2008.

[182] E. I. Unuabonah, B. I. Olu-Owolabi, K. O. Adebowale, and L. Z. Yang, "Removal of lead and cadmium ions from aqueous solution by polyvinyl alcohol-modified kaolinite clay: a novel nano-clay adsorbent," vol. 26, no. 6, 2008.

[183] R. R. Mohamed, N. A. Rizk, B. M. Abd El Hady, H. M. Abdallah, and M. W. Sabaa, "Synthesis, characterization and application of biodegradable crosslinked carboxymethyl chitosan/poly(ethylene glycol) clay nanocomposites," *Journal of Polymers and the Environment*, vol. 25, no. 3, pp. 667–682, 2017.

[184] M. Shahbazi, H. Jäger, S. J. Ahmadi, and M. Lacroix, "Electron beam crosslinking of alginate/nanoclay ink to improve functional properties of 3D printed hydrogel for removing heavy metal ions," *Carbohydrate Polymers*, vol. 240, Article ID 116211, 2020.

[185] K. R. Rajisha, B. Deepa, L. A. Pothan, and S. Thomas, "Thermomechanical and spectroscopic characterization of natural fibre composites," *Interface Engineering of Natural Fibre Composites for Maximum Performance*, pp. 241–274, 2011.

[186] M. S. H. Akash and K. Rehman, *Thermo Gravimetric Analysis. Essentials of Pharmaceutical Analysis*, Springer Nature, Berlin, Germany, 2020.

[187] N. Saadatkhah, A. Carillo Garcia, S. Ackermann et al., "Experimental methods in chemical engineering:

thermogravimetric analysis—TGA," *Canadian Journal of Chemical Engineering*, vol. 98, no. 1, pp. 34–43, 2020.

[188] T. Y. Inan, "Thermoplastic-based nanoblends: preparation and characterizations," in *Recent Developments in Polymer Macro, Micro and Nano Blends: Preparation and Characterisation*, P. M. Visakh, G. Markovic, and D. Pasquini, Eds., 1st ed., pp. 17–56, Elsevier, Amsterdam, Netherlands, 2017.

[189] A. Maleki, Z. Hajizadeh, V. Sharifi, and Z. Emdadi, "A green, porous and eco-friendly magnetic geopolymer adsorbent for heavy metals removal from aqueous solutions," *Journal of Cleaner Production*, vol. 215, pp. 1233–1245, 2019.

[190] K. Kalantari and M. Afifi, "Novel chitosan/polyvinyl alcohol/talc composite for adsorption of heavy metals and dyes from aqueous solution," *Separation Science and Technology*, vol. 53, no. 16, pp. 2527–2535, 2018.

[191] U. Malayoglu, "Removal of heavy metals by biopolymer (chitosan)/nanoclay composites," *Seperation of science and Technology*, vol. 53, 2018.

[192] A. Abdeldaym, R. F. Khedr, and R. S. Jassas, "Investigation of structural and physical properties of polypyrrole/natural clay nanocomposite as adsorbent for Zn removal," *Sustainable Chemistry and Pharmacy*, vol. 20, Article ID 100382, 2021.

[193] A. M. E. El-Aziz, K. H. Kamal, K. A. Ali, M. S. Abdel-Aziz, and S. Kamel, "Biodegradable grafting cellulose/clay composites for metal ions removal," *International Journal of Biological Macromolecules*, vol. 118, pp. 2256–2264, 2018.

[194] NanoEarth, "BET (Brunauer–Emmett–Teller)," 2017, https://nanoearth.ictas.vt.edu/access/selector/bet.html.

[195] P. Labs, "BET specific surface area," 2011, https://www.particletechlabs.com/analytical-testing/gas-adsorption-and-porosimetry/bet-specific-surface-area.

[196] R. Batool, F. Altaf, M. U. Hameed et al., "In situ chemical synthesis and characterization of PAN/clay nanocomposite for potential removal of Pb+2 ions from aqueous media," *Journal of Polymer Research*, vol. 28, no. 8, 2021.

[197] D. Abunah, C. Onindo, D. Andala, and E. Ochoti, "Physico-chemical removal of heavy metals from contaminated water using recyclable montmorillonite cellulose nanocomposite," vol. 10, pp. 1349–1361, 2019.

[198] W. Aloulou, H. Aloulou, M. Khemakhem, J. Duplay, M. O. Daramola, and R. ben Amar, "Synthesis and characterization of clay-based ultrafiltration membranes supported on natural zeolite for removal of heavy metals from wastewater," *Environmental Technology & Innovation*, vol. 18, Article ID 100794, 2020.